MEASUREMENT OF PARTICLE TEMPERATURES DURING COAL PYROLYSIS AND COMBUSTION

Guangwei Huang, Francis J. Vastola and Alan W. Scaroni

Combustion Laboratory
The Pennsylvania State University
404 Academic Activities Building
University Park, PA 16802

Introduction

The surface temperature of pyrolyzing and/or burning coal particles has been the subject of intensive investigation (1-6) because it is important in the estimation of the rate of devolatilization and/or carbon oxidation. A number of models have been established in order to predict the surface temperature of pulverized coal particles smaller than 200 μm diameter. However, few convincing models for millimeter size coal particles have emerged because of the complication of temperature gradients within the particle.

The ignition mechanism of coal particles in a hot oxidizing atmosphere is another subject of debate (5-8). Further experimental work is needed to determine whether initial ignition occurs homogeneously in the gas phase or heterogeneously at the particle surface.

The work presented here had three objectives: firstly, to develop a technique to monitor the transient temperature variations in the gas phase around a single particle during pyrolysis and/or combustion; secondly, to extrapolate the data to estimate the particle surface temperature; and thirdly, to analyze the ignition mechanism of coal and char particles.

Experimental Equipment

A schematic diagram of the equipment is shown in Figure 1. For pyrolysis studies, a flow of prepurified nitrogen was passed over copper at 673 K to remove oxygen, then through a drierite column to remove water. Dry air was used to study combustion. The reactor, a horizontal vycor tube of 8 mm internal diameter, is heated by two enclosing furnaces. The first furnace acts to preheat the in-coming gas while the second maintains the reactor at the desired temperature.

Details of the sample injection and temperature measurement systems are given in Figure 2. A single coal particle was introduced by gravity through an electromagnetically controlled injector. An electrotrigger was used to energize a 24 volt (DC) solenoid which injects the particle into the reactor.

A new approach was used to measure the transient temperature variations around the coal particle. A group of extra-fine Chromel-Alumel thermocouples with 0.05 mm diameter was employed to provide precise temperature measurement with rapid response. The thermocouples were protected by two-hole ceramic tubes. Four thermocouples were bound together using high temperature cement to form a thermocouple array (Figure 2). In order to simplify the calculation of the temperature gradient, the distance between adjacent thermocouples in the array was always the same. In this study, 0.5 and 1.0 mm spacings were used. The voltage signals generated by the thermocouple array were amplified then converted into digital signals in the data acquisition system before being sent to the microcomputer. When the particle injector was triggered, the computer was

automatically initialized to record the output of the thermocouples at 2 millisecond intervals and the data stored on disk for later analysis.

Procedure

The characteristics of the Texas subbituminous coal used are shown in Table 1. For each run a 1 mm diameter coal particle was injected into the reactor containing either preheated nitrogen or air. The bulk gas temperature was held constant at 873 K for all the experiments reported here. Before particle injection, the gas flow was stopped so that the experiments were carried out essentially in a static system. Char particles were prepared by injecting coal particles into the reactor swept by nitrogen at 873 K for 30 minutes.

Results and Discussion

The temperatures measured by the thermocouple array as a function of time, and the extrapolated surface temperatures of the single coal and char particles, are presented in Figures 3, 4 and 5 for coal pyrolysis, coal combustion and char combustion, respectively. A pyrolysis run illustrated by Figure 3 shows the temperature variations caused by the transient heat transfer between the hot gas environment and the colder coal particle. The temperature profiles illustrate the practical thermal boundary layer in the vicinity of a pyrolyzing coal particle. A rapid drop followed by a rapid increase in temperature occurred in the spherical layer 1 mm away from the particle surface while almost no temperature variation was detected 4 mm away from the particle surface.

Data for the combustion of coal and char particles are shown in Figures 4 and 5, respectively. A significant aspect of coal combustion in Figure 4 is the sudden temperature rise in the gas phase about 1.5 mm from the surface of the coal particle, compared with the much smoother curve for char combustion shown in Figure 5. Point A in Figure 4 is significant because it represents a transition from net heat loss to net heat gain by the gas. The gaseous layer surrounding the particle experienced a rapid temperature drop prior to point A and a rapid increase after this point, in contrast with the relatively smooth increase in the particle surface temperature. This implies that homogeneous ignition occurred in gas phase rather than heterogeneous ignition at the particle surface. For the experimental conditions used, the homogeneous ignition temperature was around 830 K with approximately 800 ms induction time, as represented by point A in Figure 4. This is in general agreement with the calculated results of Annamalai and Durbetaki (5). The temperture in the homogeneous combustion layer increased rapidly as the volatile matter was combusted until there was not sufficient volatile matter evolving from the particle to sustain homogeneous combustion (point B in Figure 4). The remaining and subsequently-evolved volatile matter then experienced slower oxidation with a lower heat release rate. Consequently, there was a drop in the temperature in the surrounding gas layer. Because of the need to exceed both the ignition temperature and volatile matter concentration, homogeneous combustion was observed only in the thin spherical layer about 1.5 mm from the particle surface. No rapid gas temperature rise was detected by the thermocouples closer to, or farther from, the particle surface.

Particle surface temperature and heating rate versus time are given in Figures 6 and 7, respectively. The heating rate is of interest because it is related to the rate of devolatilization and char combustion. The significance of devolatilization on combustion is seen clearly in Figures 6 and 7 which indicate that during pyrolysis the coal particle heating rate was slow and the particle temperature never exceeded the reactor temperature. In the case of devolatilized char particles a higher heating rate was observed up to the equilibrium burning

temperature of 1075 K, about 200 K higher than the reactor temperature. Figure 7 shows that coal particles had the same heating rate initially during pyrolysis and combustion until divergence at point C. This point corresponds to that of homogeneous ignition in Figure 4. After point C the heating rate was higher for combustion than pyrolysis because the heat from the homogeneous combustion reactions was transferred to the particle surface.

Two major differences existed between the char and coal during combustion. Firstly, no temperature rise in the gas was detected at any distance from the char surface (Figure 5). Secondly, the surface temperature of the char particle increased at a higher rate than that of the coal particle (Figure 6). This supports the concept of heterogeneous ignition of the char particles.

Conclusions

A fast response thermocouple array was employed to provide information on the transient heating processes associated with pyrolysis and combustion of 1 mm diameter coal and char particles at a furnace temperature of 873 K. The measured temperature variations implied that ignition occurred at the surface of the char particles but in the gas phase surrounding pyrolyzing coal particles. Homogeneous ignition occurred at 830 K causing a temperature rise in the gas in a narrow spherical layer about 1.5 mm from the surface of the coal particle.

Acknowledgements

Financial support for this work was provided by the Penn State Coal Cooperative Program. The coal was supplied by the Penn State/DOE Sample Bank and Data Base.

References

1. Field, M. A., Gill, D. W., Morgan, B. B., and Hawksley, P. G. W., Combustion of Pulverized Coal, The British Coal Utilization Research Association, Leatherhead, England (1967), p. 191.

2. Bandyopadhyay, S., and Bhaduri, D., Combustion and Flame 18, 411 (1972).

3. Howard, J. B., and Wall, T. F., Combustion and Flame 9, 377 (1965).

4. Juniper, L. A., and Durbetaki, P., Combustion and Flame 39, 69 (1980).

5. Annamalai, K., and Durbetaki, Combustion and Flame 29, 193 (1977).

6. Thomas, G. R., Stevenson, A. J., and Evans, D. G., Combustion and Flame 21, 133 (1973).

7. Gomez, C. O., and Vastola, F. J., Fuel 64, 558 (1985).

8. Stevenson, A. J., Thomas, G. R., and Evans, D. G., Fuel 52, 281 (1973).

Table 1
Characteristics of Texas Subbituminous B Coal, PSOC-423

Proximate Analysis (wt%)	As Received	Dry Basis
Moisture	24.11	
Ash	10.31	13.59
Volatile Matter	38.31	54.48
Fixed Carbon	27.27	35.93
Ultimate Analysis (wt%)		
C	47.58	62.69
H	4.01	5.29
N	0.71	0.93
S (total)	1.34	1.76
O (diff.)	11.95	15.74
Calorific Value Btu/lb (mm-Free Basis)	9836	13540

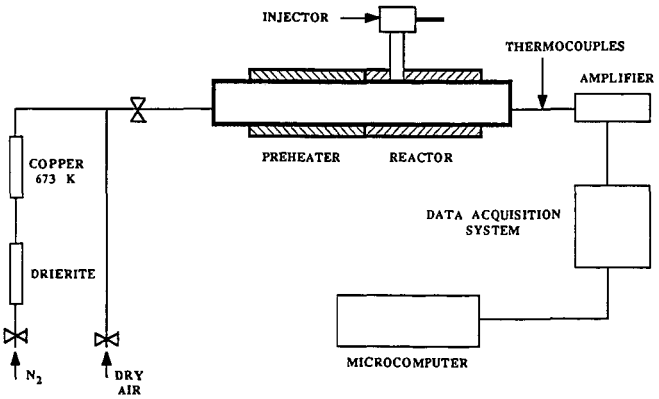

FIG. 1 SCHEMATIC DIAGRAM OF THE EQUIPMENT

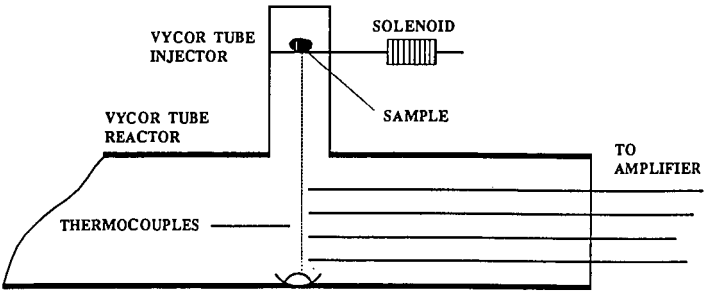

FIG. 2 INJECTION AND TEMPERATURE MEASUREMENT SYSTEM

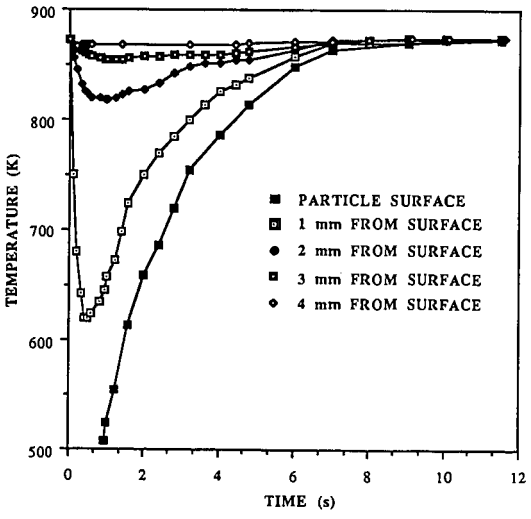

FIG. 3 TEMPERATURE HISTORY OF COAL PARTICLE SURFACE DURING PYROLYSIS

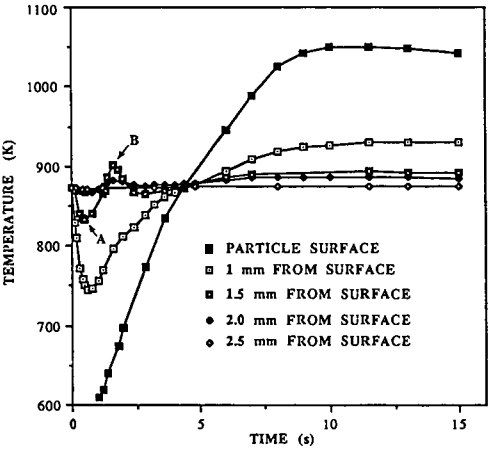

FIG. 4 TEMPERATURE HISTORY OF COAL PARTICLE SURFACE DURING COMBUSTION

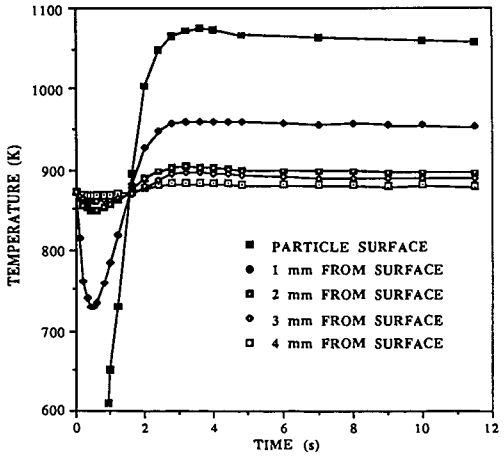

FIG. 5 TEMPERATURE HISTORY OF CHAR PARTICLE SURFACE DURING COMBUSTION

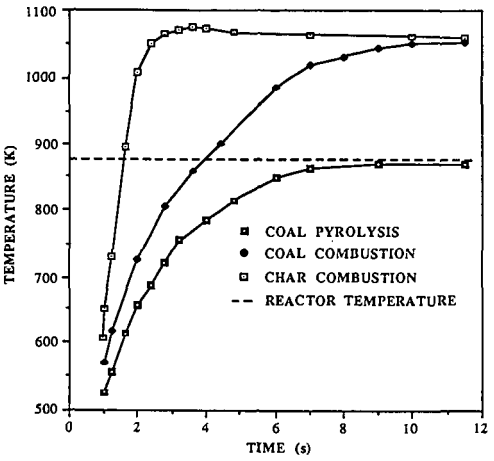

FIG. 6 TEMPERATURE HISTORY OF THE PARTICLE SURFACE

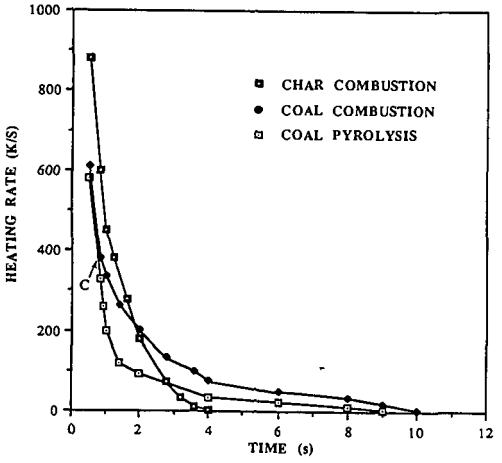

FIG. 7 HEATING RATE VERSUS TIME

INTRA-PARTICLE HEAT TRANSFER EFFECTS IN COAL PYROLYSIS

Mohammed R. Hajaligol, William A. Peters, and Jack B. Howard
Energy Laboratory and Department of Chemical Engineering,
M.I.T., Cambridge, MA 02139

May, 1987

Abstract

Time and spatial temperature gradients within pyrolyzing coal particles can exert strong effects on devolatilization behavior including apparent pyrolysis kinetics. This paper mathematically models transient spatial non-isothermalities within an isolated, spherical coal particle pyrolyzing by a single first-order reaction. The analysis provides three distinct indices of heat transfer effects by quantitatively predicting the extent of agreement between: (a) centerline and surface temperature; (b) volume averaged pyrolysis rate [or (c) volume averaged pyrolysis weight loss] and the corresponding quantity calculated using the particle surface temperature for the entire particle volume. Regimes of particle size, surface heating rate, and reaction time where particle "isothermality" according to each of criteria (a) through (c) is met to within prescribed extents, are computed for conditions of interest in entrained gasification and pulverized coal combustion, including pyrolysis under non-thermally neutral conditions.

Introduction. Many coal combustion and gasification processes involve particle sizes and surface heating rates producing temporal and spatial temperature gradients within the coal particles during pyrolysis. These gradients may strongly influence volatiles yields, compositions, and release rates, and can confound attempts to model coal pyrolysis kinetics with purely chemical rate expressions. Mathematical modelling of particle non-isothermalities is needed to predict reaction conditions (viz. particle dimension, surface heating rate, final temperature, and reaction time) for which intra-particle heat transfer limitations do not significantly influence pyrolysis kinetics, and to predict pyrolysis behavior when they do. When pyrolysis is not thermal-neutral, the analysis is non-trivial since local temperature fields are coupled non-linearly to corresponding local heat release (or absorption) rates and hence to local pyrolysis kinetics.

Much of the pertinent literature has addressed pseudo steady-state models for spatial temperature gradients within catalyst particles playing host to endo- or exothermic reactions, including, for some cases, mathematical treatment of the attendant limitations on intra-particle mass transfer of reactants or products [See Ref. (1) and references cited therein]. There appear to have been few analyses of non-isothermalities within a condensed phase material simultaneously undergoing non-thermally neutral chemical reaction(s). Previous work includes rather empirical approaches to fitting coal weight loss kinetics [see reviews by Howard (2) and Gavalas (3)], and more refined analyses of spatial non-isothermalities within exploding solids (4,5). Gavalas (2) calculated regimes of coal particle size where pyrolysis kinetics should be free of heat transfer effects, and Simmons (6) provided similar information for cellulose pyrolysis. Valuable contributions are also

emanating from the laboratories of Essenhigh (7), and Freihaut and Seery (8).

There is need for a generic, quantitative formalism to reliably predict transient intra-particle non-isothermalities and their effects on pyrolysis, as a function of operating conditions of interest in modern fuels utilization technologies. To this end the present paper presents, for an isolated spherical coal particle pyrolyzing by a single first-order reaction, quantitative predictions of three distinct indices of particle non-isothermality - namely the extent of agreement between: (1) temperatures at the particle surface and centerline; (2) the pyrolysis rate [or (3) the pyrolysis weight loss] averaged over the particle volume and the corresponding quantity calculated using the particle surface temperature for the entire particle volume. Each index is explicitly dependent on time and thus accounts for the temporal as well as the spatial non-idealities in particle "isothermality".

Method of Analysis. Spatial limitations allow only a brief summary of the theoretical approach, which is described in more detail with broader applications, by Hajaligol et al. (9). For an isolated spherical coal particle with temperature invarient thermal physical properties, pyrolyzing by a single first-order endo or exo-thermic reaction with an Arrhenius temperature dependency, heated at its surface, and transmitting heat internally only by conduction, (or by processes well-described by an apparent isotropic thermal conductivity) a standard heat balance gives the following partial differential equation for the time and spatial dependence of the intra-particle temperature field

$$\frac{1}{\alpha}\left(\frac{\partial T}{\partial t}\right) = \frac{1}{r^2}\frac{\partial}{\partial r}\left(r^2\frac{\partial T}{\partial r}\right) + \frac{(-\Delta H_{py})\,\rho\, k_0\, e^{-E/RT}}{\lambda} \qquad (1)$$

Following Boddington et al. (1982) and others, this may be rewritten in dimensionless form as

$$\left(\frac{\partial \theta}{\partial \tau}\right) = \frac{1}{\xi^2}\frac{\partial}{\partial \xi}\left(\xi^2\frac{\partial \theta}{\partial \xi}\right) + \delta \exp\left[\frac{\theta}{\beta + \varepsilon\theta}\right] \qquad (2)$$

Symbols are defined in the nomenclature section at the end of the paper. Solution of Equation (1) or (2) requires specification of one initial condition and two spatial boundary conditions. The initial condition prescribes the temperature field throughout the coal particle at the instant heating begins

$$T(r,0) = T_o \qquad (3)$$

or

$$\theta(\xi,0) = 1 \qquad (4)$$

One boundary condition is the mathematical expression for centerline symmetry of the particle temperature field at all pyrolysis times

$$\left(\frac{\partial T}{\partial r}\right)_{r=0} = 0 \tag{5}$$

or

$$\left(\frac{\partial \theta}{\partial \xi}\right)_{\xi=0} = 0 \tag{6}$$

Four cases are of interest for the second boundary condition in the present analysis:

(1) A finite rate of heat transmission to the particle surface describable in terms of an apparent heat transfer coefficient

$$-\lambda\left(\frac{\partial T}{\partial r}\right)_{r=R_0} = h_{eff}\left(T - T_\infty\right) \tag{7}$$

or

$$\left(\frac{\partial \theta}{\partial \xi}\right)_{\xi=1} = -N_{Bi}\left(\theta - \theta_\infty\right) \tag{8}$$

This case would be applicable to heating of coal particles in a fluidized bed or by molecular conduction from a high temperature gas. It also automatically accommodates cases where the overall rate of heat transfer to the particle is influenced by extra-particle resistance [i.e. cases of non-infinite Biot number].

(2) A prescribed constant rate of increase in the particle surface temperature:

$$T_s(t) = T_0 + \dot{m}\, t \tag{9}$$

or

$$\theta_s(\tau) = 1 - \gamma\, \tau \tag{10}$$

This case is applicable to screen heater reactors or other apparatus where surface heating rates are maintained essentially constant.

(3) A known, constant surface heat flux density:

$$-\lambda\left(\frac{\partial T}{\partial r}\right)_{r=R_0} = \dot{q}_0/4\pi R_0^2 \tag{11}$$

or

$$\left(\frac{\partial \theta}{\partial \xi}\right)_{\xi=1} = -\Phi \tag{12}$$

This case is especially applicable to fires and furnaces under conditions where the particle surface temperature remains well below the temperature of the surroundings, and sample heating is dominated by radiation.

(4) A special limiting case of (1) through (3) above is an infinitely rapid surface heating rate:

$$T_s(t) = T_s(\infty) \quad , \qquad r = R_o \tag{13}$$

or

$$\theta_s(\tau) = 0 \quad , \qquad \xi = 1 \tag{14}$$

This case would approximate the heat transfer characteristics of systems providing very rapid surface heating of the coal particles, for example shock tubes, laser and flash lamp reactors, and coal dust explosions, where surface heating rates are estimated to exceed 10^5 - 10^7 C/s.

Equations (1) and (2) were solved numerically for each of the above four cases of boundary condition, using a procedure based on the method of lines and on Gear's method. Only our results for constant surface heating rate, Case (2) above, will be presented here. Results for other cases are presented by Hajaligol et al. (9).

The solutions to these two equations are predictions of the spatial variation of the intra-particle temperature field with pyrolysis time. This information was used to compute three distinct indices of particle non-isothermality:

(1) The extent of agreement between the surface and centerline temperature of the particle:

$$\eta_T(t) = \left[T_s(t) - T_{cL}(t) \right] \Big/ T_s(t) \tag{15}$$

or

$$\hat{\eta}_T(\tau) = \theta_{cL}(\tau) - \theta_s(\tau) \tag{16}$$

(2) A time dependent effectiveness factor for pyrolysis rate, defined as the ratio of: the local pyrolysis rate averaged over the particle volume, to the pyrolysis rate calculated using the particle surface temperature for the entire particle volume:

$$\eta_r(t) = \frac{\frac{1}{V}\int_V k_o e^{-E/RT(r,t)}\, dV}{k_o e^{-E/RT_s(t)}} \tag{17}$$

or

$$\hat{\eta}_r(\tau) = \frac{3\int_0^1 k_o e^{-\frac{\beta}{\beta\varepsilon+\varepsilon^2\theta}(\xi,\tau)}\, \xi^2 d\xi}{k_o e^{-\beta/(\beta\varepsilon+\varepsilon^2\theta_s(\tau))}} \tag{18}$$

(3) A time-dependent effectiveness factor for overall pyrolytic conversion (i.e. weight loss or total volatiles yield) defined as the ratio of: the volume averaged weight loss, to the weight loss calculated using the particle surface temperature for the entire particle volume:

$$\eta_c(t') = \frac{1 - \frac{1}{V}\int_V \left\{ \exp\left[-\int_0^{t'} k_0 e^{-E/RT(V,t)} dt \right] \right\} dV}{1 - \left\{ \exp\left[-\int_0^{t'} k_0 e^{-E/RT_s(t)} dt \right] \right\}} \qquad (19)$$

or

$$\hat{\eta}_c(\hat{\tau}) = \frac{1 - 3\int_0^1 \left\{ \exp\left[-\int_0^{t'} \phi e^{-\beta/[\varepsilon\beta + \varepsilon^2\theta(\xi,\tau)} d\tau \right] \right\} d\xi}{1 - \left\{ \exp\left[-\int_0^{t'} \phi e^{-\beta/[\varepsilon\beta + \varepsilon^2\theta_s(\tau)} d\tau \right] \right\}} \qquad (20)$$

Results and Discussion. The above analysis was used with boundary condition (2) [constant surface heating rate] to predict effects of various pyrolysis parameters on $\eta_T(t)$, $\eta_r(t)$, and $\eta_c(t)$ as a function of pyrolysis time. Unless otherwise stated the following values of thermal physical and chemical properties of the coal were employed: ρ = 1.3 g/cm^3, λ = 0.0006 cal/cm-s-C, C_p = 0.4 cal/g-C, ΔH_{py} = 0 cal/g, k_o = 10^{13} s^{-1}, and E = 50 kcal/g-mole. Effects of non-zero heats of pyrolysis are discussed later in the paper.

Figures 1 - 3 respectively show the effects of particle size on $\eta_T(t)$, $\eta_r(t)$, and $\eta_c(t)$, for a surface heating rate and final temperature of 10^4 C/s and 1000 C. For particle sizes > 50 μm, the time to relax internal temperature gradients [i.e. for $\eta_T(t)$ to decline from its maximum value to about zero] increases with roughly the square of particle diameter as expected. Initially the spatial non-idealities in temperature (Fig. 1) increased with increasing pyrolysis time, because the time for the surface to reach the final temperature [$T_{s,f}$/m] is much less than the particle thermal response time, and the intra-particle temperature field is unable to keep pace with the rapidly rising surface temperature. The magnitude and duration of this initial temperature transient increases with particle diameter, because the particle thermal response time increases with particle size.

The rate index of non-isothermality, $\eta_r(t)$ (Figure 2) tracks the non-idealities in particle temperature. For a given particle size and thermally neutral reactions $\eta_r(t)$ indicates spatially non-isothermal kinetic behavior [i.e. $\eta_r(t) < 1$] over a broader range of pyrolysis times than does $\eta_T(t)$ [i.e. for which $\eta_T(t) > 0$, Fig. 1]. The rate index expresses the influence of the temperature non-idealities on the predicted volume averaged pyrolysis rates via an exponential function. Thus an amplification of the magnitude and duration of the temperature non-idealities is not surprising. Furthermore, when volatiles release rates are of interest, $\eta_r(t)$ is clearly a more reliable index of particle non-isothermality than is $\eta_T(t)$.

The conversion index of non-isothermality, $\eta_c(t)$ (Fig. 3), reflects the non-idealities in rate, and the exponential increase in conversion with total pyrolysis time. The latter effect attenuates the former at short and long pyrolysis times by respectively, denying and supplying the reaction adequate time to attain completion at the imposed heating rate. Thus for each particle size there is an intermediate range of reactions times throughout which the strong non-idealities in pyrolysis rate (Fig. 2) contribute major non-idealit-

ies in conversion (Fig. 3). The exponential dependencies of conversion on rate and reaction time, also cause the magnitude of $\eta_x(t)$ to change rapidly with pyrolysis time, resulting in the sharp variations in this index depicted in Fig. 3. Clearly, in light of the differences in Figures 1 through 3, when total volatiles yield is of interest, $\eta_x(t)$ is the preferred index of non-isothermality over either $\eta_T(t)$ or $\eta_r(t)$.

Figure 4 shows that at a fixed particle size, increasing the surface heating rate increases the magnitude but decreases the duration of the initial non-idealities in the particle temperature field. The first effect arises because, with increasing surface heating rate, the surface temperature increases so rapidly during a time equal to the thermal response time of the particle, that the intra-particle temperature field lags further and further behind the surface temperature. The shorter relaxation time arises because the higher initial temperature gradients generated at higher surface heating rates cause a more rapid attenuation of the initial disturbance. With increasing heating rate, these sharp initial intra-particle temperature gradients translate into strong non-idealities in the local pyrolysis rates and hence into significant departures of $\eta_r(t)$ from unity (Fig. 5). With declining heating rates (Fig. 5) the magnitude of these non-idealities is attenuated but they remain significant over increasing ranges of pyrolysis time. These effects respectively arise because decreasing the surface heating rate reduces the differences between the surface and internal temperatures (Fig. 4), and because the resulting intra-particle temperature gradients are lower, and thus provide less driving force for temperature relaxation, thereby extending the time over which the intra-sample pyrolysis rates exhibit significant non-idealities. Increasing particle size at a fixed heating rate exacerbates each of the above effects (Fig. 2).

The impacts of these intra-sample rate variations on the conversion index of non-isothermality $\eta_x(t)$, are attenuated strongly in both magnitude and duration (Fig. 6), due to the interplay of rate and cumulative pyrolysis time discussed above. The magnitude of the non-idealities in $\eta_x(t)$ are worsened with increasing heating rate, because surface temperature and surface pyrolysis rate more and more rapidly outpace the corresponding quantities within the particle, thus expanding the differences between the extents of conversion predicted for these two regions at smaller and smaller reaction times. Conversely, the non-idealities in $\eta_x(t)$ decrease when heating rate decreases, because the particle temperature field (Fig. 4), and average pyrolysis rate (Fig. 5), track the surface temperature more and more closely, and because the greater time required for the surface temperature to attain its final value, allows intra-particle conversion to proceed further to completion.

For a thermally neutral reaction, a change in the activation energy for pyrolysis has no effect on intra-particle temperature gradients [and hence on $\eta_T(t)$], but Figure 7 shows that increasing E increases the magnitude of the non-idealities in $\eta_r(t)$, as would be expected since larger E's imply stronger dependencies of rate on temperature. Since $\eta_T(t)$ is unaffected by changing E, any effect of E on $\eta_x(t)$ will reflect only E-induced changes in $\eta_r(t)$. Such effects should be small since at this heating rate (10^3 C/s) quite large changes in $\eta_r(t)$ at an E of 50 kcal/g-mole (Fig. 5), are strongly attenuated in $\eta_x(t)$ (Fig. 6), and the E-induced variations in $\eta_r(t)$ (Fig. 7) are by comparison, rather small.

Figure 8 shows that for constant ρ and C_p, decreasing either the thermal conductivity or thermal diffusivity of the coal increases the magnitude and duration of non-idealities in $\eta_r(t)$ and $\eta_c(t)$. For an endothermic reaction the values of $\eta_T(t)$ and $\eta_r(t)$ at long pyrolysis times would increase with increasing values of either of these thermal parameters. For example, for $\Delta H_{py} \simeq +50$ cal/g coal, these two indices would increase by a factor of 10, for 10 to 15% increases in α or λ (Hajaligol et al. 1987).

Figure 9 shows the effects of pyrolysis time on $\eta_T(t)$, $\eta_r(t)$, and n(t) for cases where pyrolysis is not thermal neutral. The discussion is simplified by expressing the results in terms of a dimensionless parameter δ, which reflects the interaction of chemical kinetic and thermal physical parameters in determining the impact of chemical enthalpy on particle non-isothermality. Delta is derived by non-dimensionalizing Eq. (1), see Eq. (2), and physically can be thought of as the ratio of the average rate of heat generation (or depletion) at the particle surface from pyrolysis, to the average rate of conductive transfer of heat into the particle from its surface. Figure 9 shows that for reasonable exo- or endo-thermicities, $\eta_T(t)$ and $\eta_r(t)$ do not approach perfect ideality, even at long pyrolysis times, while $\eta_c(t)$ goes virtually to unity (isothermal behavior) in reasonable times. The magnitude and duration of the non-idealities expressed by $\eta_c(t)$ depend on the ratio of the pyrolysis time to the particle heat-up time (Hajaligol et al. 1987). At long pyrolysis times $\eta_T(t)$ and $\eta_r(t)$ attain δ-specific plateaus that are independent of heating rate or particle size, although both parameters affect the magnitude and duration of the transients in these two indices.

Figure 10 shows, for thermally neutral pyrolysis, domains of particle size and surface heating rate where the particle is at least 95% "isothermal" according to each of the above indices [$\eta_T(t)$, $\eta_r(t)$, and $\eta_c(t)$]. The temperature index provides a broader range of compliant particle sizes and heating rates, because it is uninfluenced by devolatilization kinetics. For a non-thermally-neutral reaction it is much more difficult to define domains of particle size and heating rate where $\eta_T(t)$ meets the 95% ideality criterion - note the very small δ values required for $\eta_T(t)$ to approach 0 in Fig. 9.

The rate index [$\eta_r(t)$] obviously enfolds kinetic effects, and consequently presents a more narrow domain of isothermality (Fig. 10). Clearly this index, rather than $\eta_T(t)$ alone, should be considered in evaluating the role of heat transfer effects in devolatization kinetic data and in designing experiments to probe intrinsic chemical rates. The conversion index, $\eta_c(t)$, provides a somewhat broader isothermality domain, due to the damping effect of pyrolysis time discussed above.

Effects of activation energy and thermal physical properties on the isothermality domains can be inferred from Fig.'s 7 and 8 respectively. Increasing or decreasing E as in Fig. 7, has no effect on the regions prescribed by $\eta_T(t)$ and $\eta_c(t)$, but respectively decreases and increases the domains defined by $\eta_r(t)$ (dashed lines of Fig. 10).

When pyrolysis is not thermally neutral, the domains of particle isothermality may, depending on the magnitude of ΔH_{py}, shrink from the boundaries defined in Fig. 10. Regimes of D_p and $\dot{m}$ meeting each of the above criteria can still be prescribed by calculating compliant families of curves in Fig. 10, using ΔH_{py} as a parameter. Alternatively, the parameter δ can be used to

advantage in a more efficient computation procedure that accounts explicitly for all parameters contributing to heat of pyrolysis effects. The rate index, $\eta_r(t)$ shows the greatest effect of ΔH_{py} (Fig. 9). Figure 11 shows how $\eta_r(t)$ varies with $|\delta|$, where the upper and lower branches [$\eta_r(t) > 1$, and < 1], reflect exo- and endo-thermic pyrolysis, respectively. This figure is used to obtain values of δ such that $\eta_r(t)$ indicates a desired extent of isothermality, say 95%. With δ fixed, and fixed thermal-physical properties, the particle diameter, D_p, final surface temperature T_s, and surface heating rate, m, become the only adjustable parameters of the system. For preselected particle diameters, Fig. 10 is then used to define the allowed maximum surface heating rates for any of the isothermality indices, and the value from Fig. 11 sets the corresponding maximum allowed surface temperature. Alternatively a desired surface heating rate can be pre-selected with the corresponding maximum allowed particle diameter and surface temperature being obtained from Figs. 10 and 11 (via δ) respectively, or a maximum surface temperature can be pre-chosen with the compliant δ value (Fig 11) prescribing the maximum allowed D_p, and Fig. 10 the corresponding maximum acceptable surface heating rate. This protocol is conservative in that it is valid for all pyrolysis times, and utilizes the most stringent of the above isothermality indices, $\eta_r(t)$.

Conclusions

1. The extent of coal particle non-isothermality at any stage of pyrolysis can be quantitatively depicted in terms of numerical indices reflecting not only spatial non-uniformities of the intra-particle temperature field, but also non-idealities in the rate and extent of pyrolysis.

2. Mathematical modeling of coupled rates of intra-particle pyrolysis and heat transmission, relates each index to operating conditions of interest in coal combustion and gasification including surface heating rate, particle diameter, final temperature, and pyrolysis time.

3. Domains of surface heating rate and particle diameter where each isothermality criterion is met to within 5% at all pyrolysis times are plotted for a base case of zero heat of pyrolysis.

4. Data and procedures for using these same isothermality maps when pyrolysis is not thermal neutral are also provided.

5. The analysis shows that diagnosing a pyrolyzing coal particle as "isothermal" based upon close agreement between its surface and centerline temperature, can lead to serious errors in estimates of corresponding volatiles release rates and total volatiles yields.

6. Each isothermality index exhibits significant temporal variations, showing that pyrolysis time, and hence extent of conversion must be considered in assessing particle non-isothermality and its impact on pyrolysis behavior.

Nomenclature

d_p	Particle Diameter, Cm
E	Activation Energy, Cal/g-mole
h_{eff}	Effective Heat Transfer Coefficient, Cal/(Cm²-Sec-C)
k_o	Reaction Frequency Factor, sec⁻¹
$\dot{m}$	Surface Heating Rate, °K/sec
N_{Bi}	Biot Number; $h_{eff}\, d_p / 2\lambda$
$\dot{q}$	Surface Heat Flux Density, Cal/sec
R	Gas Constant; 1.987 Cal/gmole°K
r	Radius, Cm
R_o	Partice Radius, Cm
T	Temperature, °K
T_o	Initial Temperature, °K
T_s	Surface Temperature, °K
$T_{s,f}$	Final Surface Temperature, °K
T_∞	Ambient Temperature, °K
t	Time, Sec
V	Particle Volume, Cm³
ρ	Particle Density, g/cm³
λ	Particle Thermal Conductivity, Cal/(Cm-Sec-C)
α	Particle Thermal Diffusivity, Cm²/Sec
ΔH_{py}	Heat of Pyrolysis, Cal/g
θ	Dimensionless Temperature; $\frac{T - T_{s,f}}{T_o - T_{s,f}}$
θ_s	Dimensionless Surface Temperature; $\frac{T_{s(t)} - T_{s,f}}{T_o - T_{s,f}}$
θ_{CL}	Dimensionless Center Temperature; $\frac{T_{CL(t)} - T_{s,f}}{T_o - T_{s,f}}$
θ_∞	Dimensionless Ambient Temperature; $\frac{T_\infty - T_{s,f}}{T_o - T_{s,f}}$
τ	Dimensionless Time; $\alpha t / R_o^2$
ξ	Dimensionless Length; r/R_o

$\eta_T, \hat{\eta}_T$ Dimensionless Temperature Index

$\eta_r, \hat{\eta}_r$ Dimensionless Rate Index

$\eta_c, \hat{\eta}_c$ Dimensionless Conversion Index

ε Dimensionless Parameter; $R T_{s,f} / E$

β Dimensionless Parameter; $R T_{s,f}^2 / E (T_o - T_{s,f})$

δ Dimensionless Parameter; $(-\Delta H_{py}) \rho d_p^2 k_o e^{-E/R T_{s,f}} / [4 \lambda (T_o - T_{s,f})]$

γ Dimensionless Heating Rate; $\dot{m} d_p^2 / [4 \alpha (T_o - T_{s,f})]$

Φ Dimensionless Heat Flux Density; $\dot{q}'' / [2\pi \lambda d_p (T_o - T_{s,f})]$

Acknowledgements

Prime U.S.D.O.E. support for this work was provided via Contract No. DE-AC22-84PC70768, from the AR & TD Combustion Program of the Pittsburgh Energy Technology Center. Additional U.S.D.O.E. support was provided under Contract No. DE-AC21-85MC222049, from the Advanced Gasification Program of the Morgantown Energy Technology Center.

References

1. Froment, G. F., and K. B. Bischoff, Chemical Reactor Analysis & Design, John Wiley and Sons, 1979.

2. Howard, J. B., Fundamentals of Coal Pyrolysis and Hydropyrolysis, in Chemistry of Coal Utilization, 2nd Suppl. Vol., Wiley NY 1981.

3. Gavalas, G. R., Coal Pyrolysis, Elsevier Scientific Pub., 1982.

4. Boddington, T., P. Gray, and S. K. Scott, J. Chem. Soc., Faraday Trans. 2, 78, 1721-1730, 1982.

5. Scott, S. K., T. Boddington, and P. Gray, Chem. Eng. Science, Vol. 39, No. 6, 1079-1085, 1984.

6. Simmons, G.M., Am. Chem. Soc., Div. of Fuel Chem. Preprints, April 1984.

7. Essenhigh, R.H., Dept. of Mechanical Eng., Ohio State University, Work in Progress, 1987.

8. Seery, D. J., J. D. Freihaut, and W. M. Proscia, Technical Progress Reports for DOE, 1985-1986, United Technologies Research Center, E. Hartford, CT.

9. Hajaligol, M. R., J. B. Howard, and W. A. Peters, Predicting Temporal and Spatial Non-Isothermalities within Reacting Condensed Phase Media, To be Submitted to the AIChE journal, 1987.

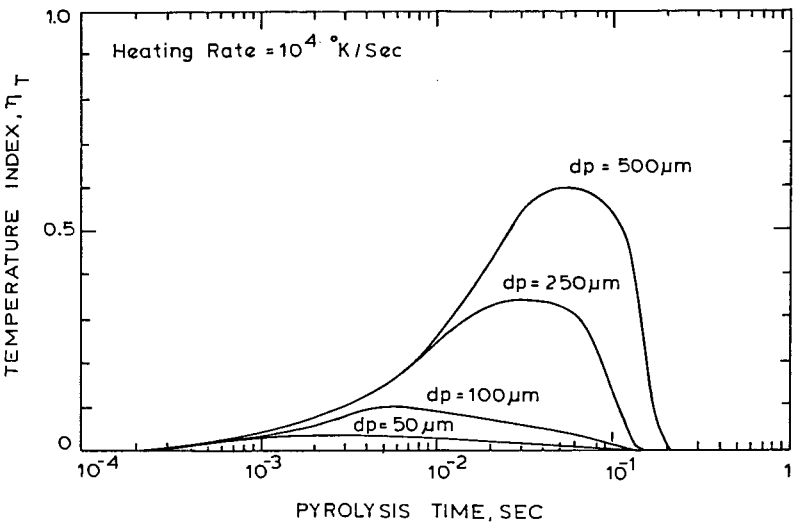

Figure 1. Effects of Particle Diameter on the Temperature Index at 10^4 K/sec Heating Rate.

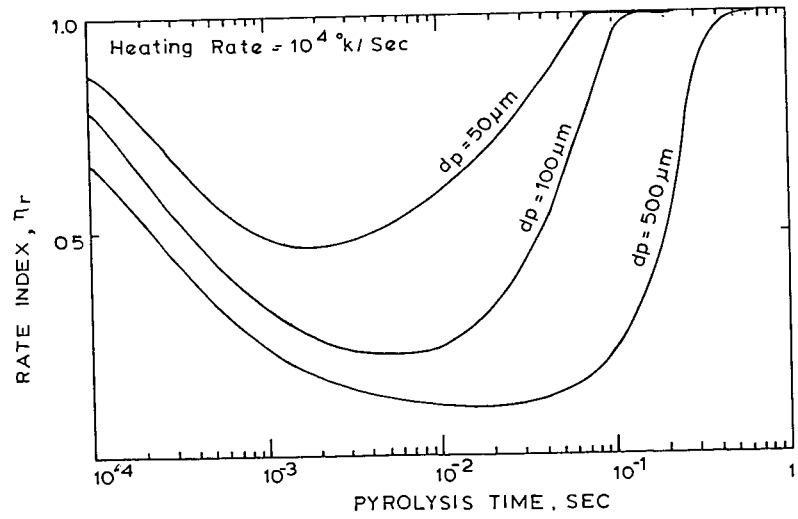

Figure 2. Effects of Particle Diameter on the Rate Index at 10^4 K/sec Heating Rate.

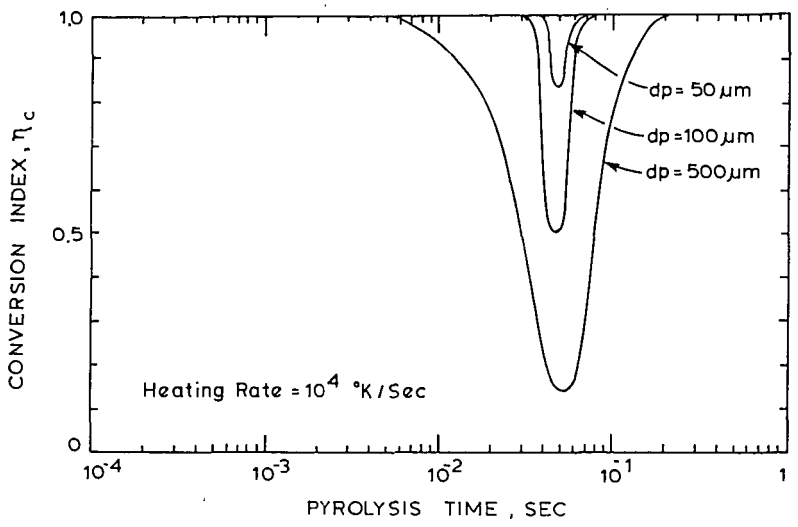

Figure 3. Effects of Particle Diameter on the Conversion Index at 10^4 K/sec Heating Rate.

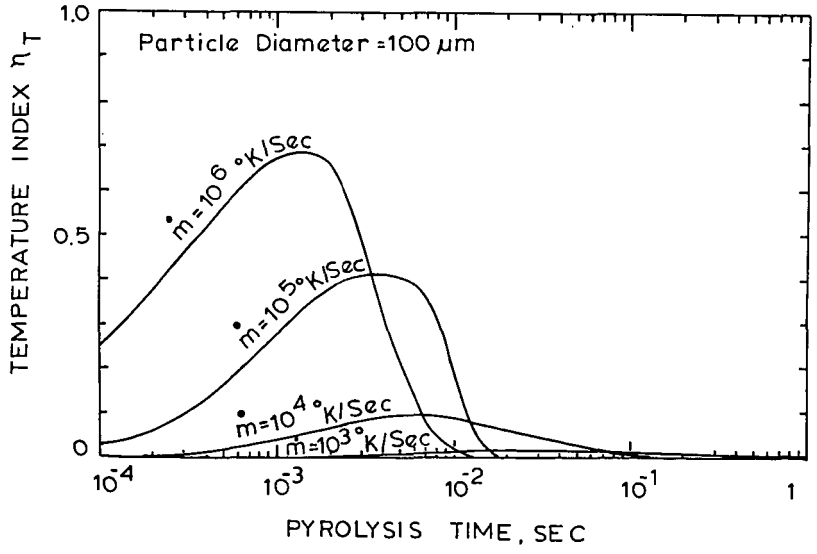

Figure 4. Effects of Heating Rate on the Temperature Index for 100 mm Particle Diameter.

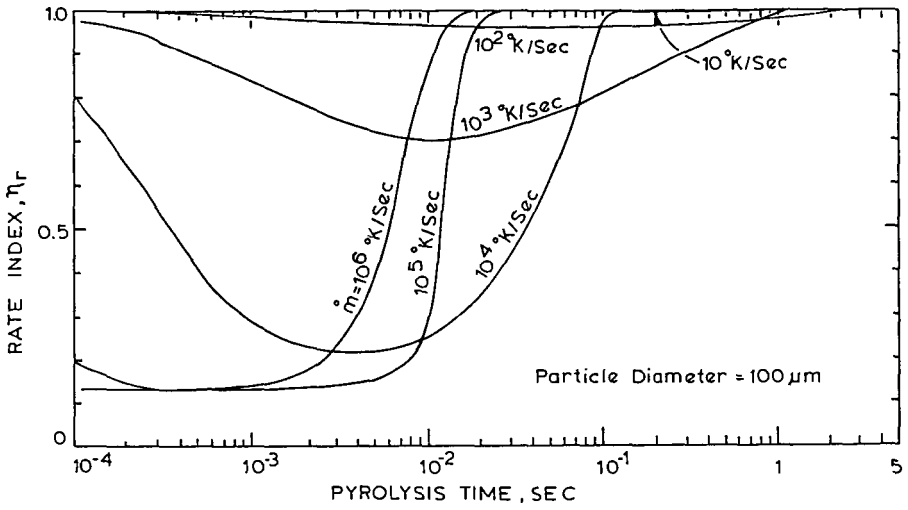

Figure 5. Effects of Heating Rate on the Rate Index for 100 mm Particle Diameter.

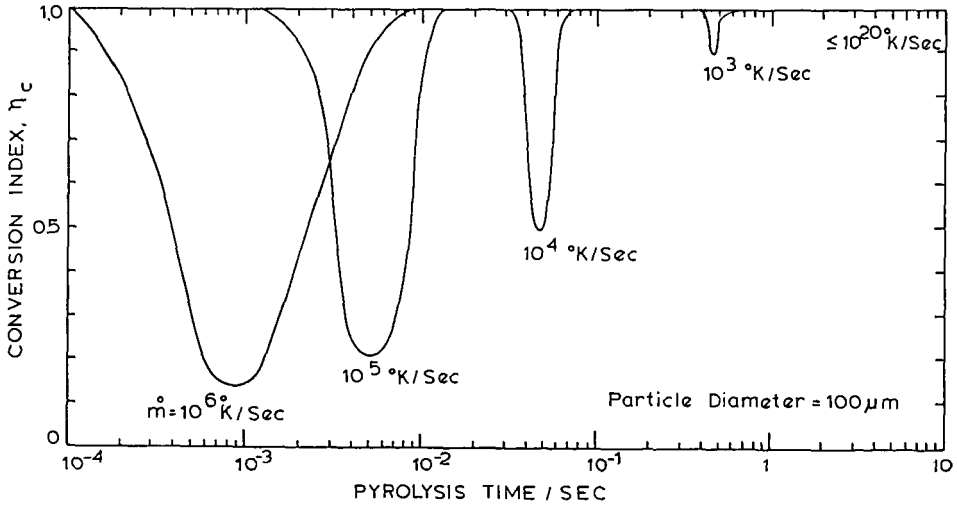

Figure 6. Effects of Heating Rate on the Conversion Index for 100 mm Particle Diameter.

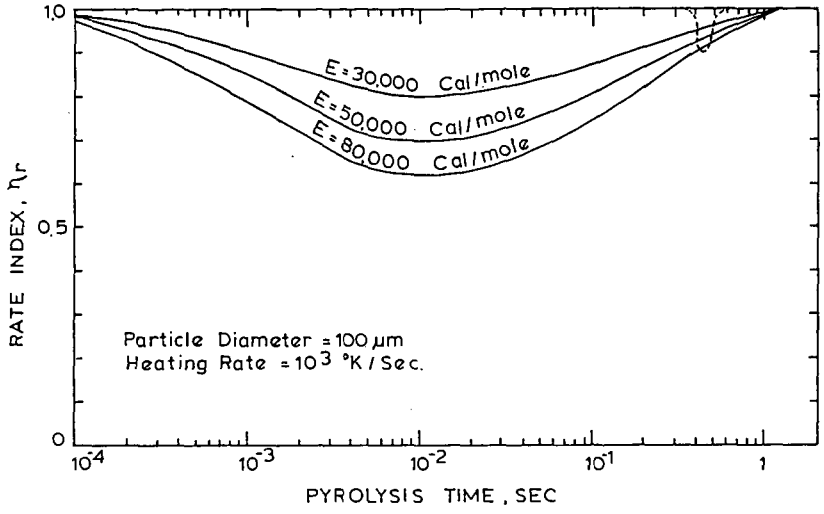

Figure 7. Effects of Activation Energy on the Rate and Conversion Indices.

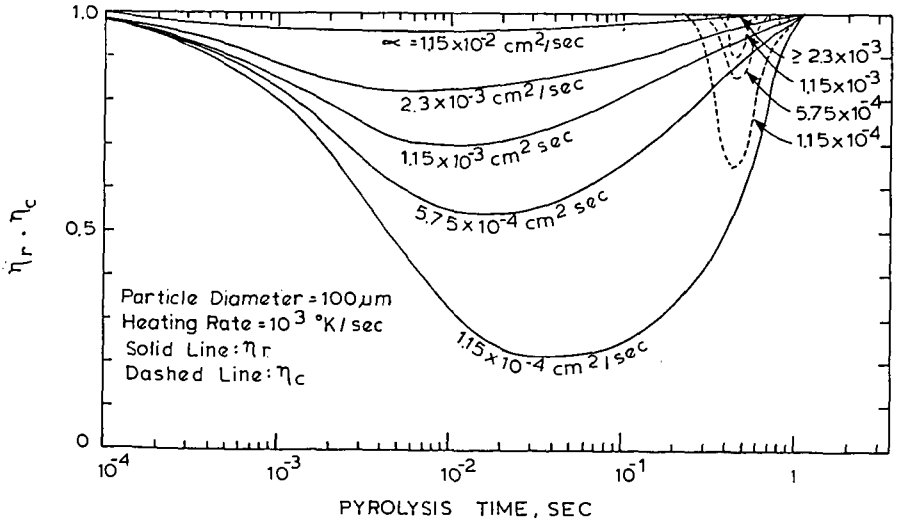

Figure 8. Effects of Thermal Diffusivity on Rate and Conversion Indices.

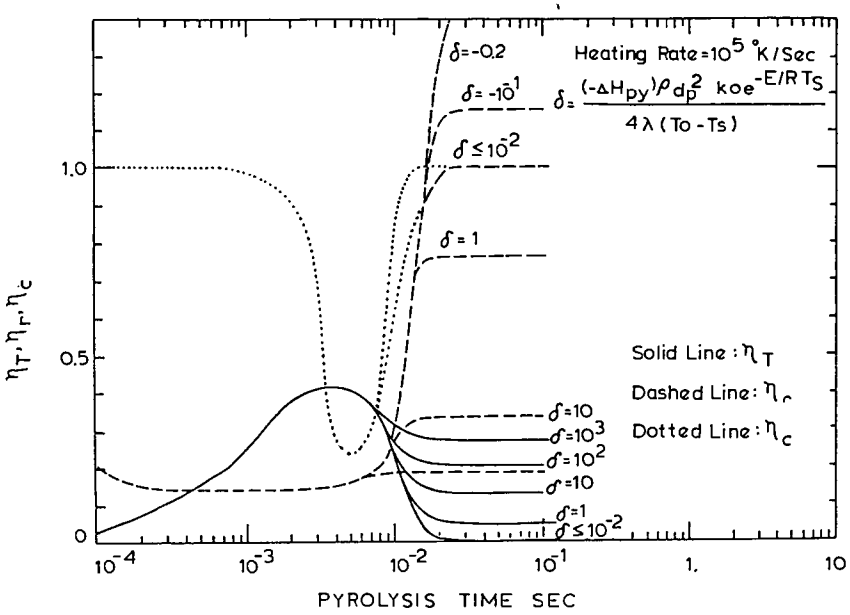

Figure 9. Effects of Heat of Pyrolysis on Indices.

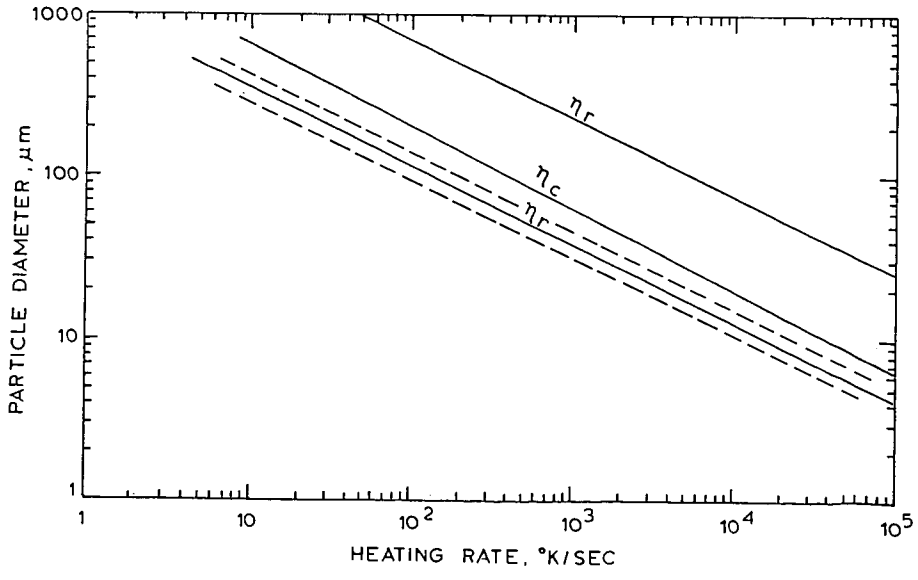

Figure 10. Isothermal Regions Defined by Different Indices.

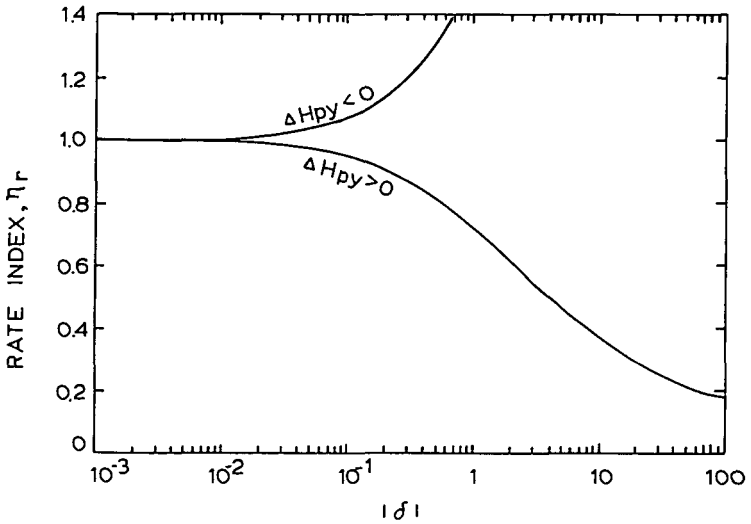

Figure 11. Effects of Heat of Pyrolysis on the Spatial Value of Rate Index.

THERMOKINETIC TRANSPORT CONTROL AND STRUCTURAL MICROSCOPIC REALITIES IN COAL AND POLYMER PYROLYSIS AND DEVOLATILIZATION: THEIR DOMINANT ROLE IN DUST EXPLOSIONS

By M. Hertzberg, I. A. Zlochower, R. S. Conti, and K. L. Cashdollar

U. S. Bureau of Mines
Pittsburgh Research Center
P.O. Box 18070
Cochrans Mill Road
Pittsburgh, PA 15236

ABSTRACT

The reaction mechanism for coal pyrolysis and devolatilization involves the inward progression from the exposed surface of a decomposition wave, whose speed of propagation determines the pyrolysis rate. The speed is controlled by the heat flux driving the wave and by thermodynamic transport constraints within the particle. Microscopic data are presented that reveal the structure of that wave front for unidirectional laser exposure of both macroscopic coal samples and microscopic dust particles. At burner-level heat fluxes of 100 to 125 W/cm^2, the wave front thickness is less than 50 μm.

New data are also presented for polymethylmethacrylate (PMMA) at flux levels of 12-115 W/cm^2 that give a pyrolysis and devolatilization "rate coefficient" of,

$$k_t = \{\int_{T_o}^{T_s} C(T)dT + \Delta H_v\}^{-1} ,$$

whose value is predictable from thermodynamic transport constraints alone. Except for the complication of the coal's char-layer residue and its increasing thickness, which insulates the wave front from the heat source flux that drives it, both coal and PMMA behave similarly. For PMMA, the decomposition temperature, T_s, is 350-400° C; for coal it is 450-600° C.

There is no substantive evidence to support the traditional viewpoint that the reaction processes occur isothermally under chemical rate control and that they are describable by unimolecular, Arrhenius functions of the source temperature.

The volatility yield of a dust and its rate of devolatilization play dominant roles in the overall mechanism of flame propagation in dust-air mixtures. Data for the particle size dependences of the lean limits of flammability for coals and polymers reveal those roles. The above measured rate coefficient for PMMA gives a reasonable prediction of the coarse size at which the particle devolatilization process becomes rate limiting in a PMMA dust explosion.

INTRODUCTION

Two theories or models have been used to describe the process of coal particle pyrolysis and devolatilization. The first is the traditional viewpoint, which considers the reaction process to be under chemical rate control (1, 2, 3); the second is a newer viewpoint that considers the reaction process to be under heat transport control (4, 5, 6, 7). In the traditional model the reaction or reactions are viewed as occurring isothermally throughout the particle and are described by classical, unimolecular, Arrhenius functions of the particle temperature, T. The reaction rate is given by

$$\frac{d\,V(t)}{dt} = k_o\,[e^{-E_a/RT}]\,[V(\infty) - V(t)], \qquad 1)$$

where V(t) is the volatile yield (in pct) after an exposure time, t; $V(\infty)$ is the maximum volatile yield as $t \to \infty$; k_o is the preexponential factor; E_a is the activation energy; R is the universal gas constant; and T is the temperature of the pyrolyzing particle. Considerable effort has gone into the development of complex, parallel or sequential reaction schemes to predict the overall rate of pyrolysis and the yields of volatile products. Surprisingly, however, little effort has been devoted to a realistic analysis of the heat transport processes by which particle temperatures, initially at T_o, are elevated to the reaction temperature T after

their exposure to some high temperature source at T_h. Early researchers generally assumed that the exposed coal particles rapidly reached the high temperatures of the furnace walls, or the hot gases, or the electrically-heated screens to which they were exposed. The temperature used in Equation 1 was generally the source temperature, T_h. A major exception was Zielinski (7), whose independent analysis of the data of many investigators led to the conclusion that the rate of the heat transfer from the high-temperature source to the coal particles exerted the dominant influence on the rate of volatiles evolution. He noted that coal particle temperature measurements were "very rare indeed," and cautioned researchers against assigning "the temperature of the heat carrier or the container walls" to the temperature of "the coal particles themselves." Zielinski's analysis was generally ignored until the more recent studies of Freihaut and Vastola (8), and the reanalysis of particle pyrolysis data by Solomon and coworkers (9, 10). Using direct optical measurements of particle temperatures, Solomon et al. (10) showed clearly that, during pyrolysis, T was generally much lower than T_h. For example, in an entrained flow reaction at a source temperature of T_h = 1300° C, coal particles of 45-75 μm diameter were completely devolatilized by the time they had reached temperatures of only 700-800° C. Their analysis is nevertheless limited to the problem of heat transfer to the particle; the particle itself is still treated as reacting isothermally, and uniformly throughout its extent. Internal variations in temperature and reaction rate are ignored. Since, however, the particle is not isothermal, one must go even further in the reanalysis. For coal, especially, there is inevitably a hotter, opaque char layer at the surface of the particle that surrounds and conceals the lower temperature region of active pyrolysis further within the particle.

Accordingly, not only must one consider heat transport limitations to the particle from the external heat source, but also heat transport limitations within or through the particle; that is, from its surface to its interior. Attempts to address that limitation lead to the newer viewpoint or model. The situation in its simplest form is depicted in Figure 1, and the newer theory simply applies the First Law of Thermodynamics to the system. A planar coal surface is depicted, pyrolyzing and devolatilizing at a steady-state rate, $\dot{x}_o$, in an incident radiative source flux of intensity, I. The system depicted is coal, which is complicated by a char residue above the pyrolysis reaction zone. Initially, it will be simpler to assume that the reactant is one that devolatilizes completely so that the incident flux is absorbed directly at the devolatilizing surface. Polymethylmethacrylate (PMMA) is an example of such a substance. A fraction of the incident flux, rI, is reflected, and another portion, I_ℓ, is lost to the colder surroundings by conduction, convection, and reradiation. For the steady-state propagation of the pyrolysis wave, at the liner rate, $\dot{x}_o$, the First Law requires that the net absorbed flux, $I_{abs} = I(1-r)-I_\ell$, first supply the power necessary to bring each element of the solid reactant with its heat capacity C(T) to the reaction zone or decomposition temperature, T_s, from its initial temperature, T_o; and second, supply the heat of devolatilization. Thus,

$$I_{abs} = I(1 - r) - I_\ell = \dot{x}_o \rho [\int_{T_o}^{T_s} C(T)dT + \Delta H_v]. \qquad 2)$$

Solving for the mass devolatilization rate per unit area gives

$$\dot{m} = \dot{x}_o \rho = k_t I_{abs} = [\int_{T_o}^{T_s} C(T)\, dT + \Delta H_v]^{-1} I_{abs}, \qquad 3)$$

where the rate coefficient, k_t, is given by the reciprocal of the net enthalpy change for the overall heating and devolatilization process.

This newer viewpoint should be contrasted with the traditional one. In this flux-driven, heat-transport-limited model (Equations 2 and 3), once the input flux level exceeds some critical value for the onset of reaction, which is the loss flux, the predicted rate is not particularly sensitive to the reaction zone temperature of the pyrolyzing surface. That temperature, T_s, is only the upper bound of a heat capacity integral. The rate coefficient, k_t, is much more sensitive to the heat of devolatilization or vaporization, ΔH_v. By contrast, in the traditional viewpoint (Equation 1), the reaction temperature T is the only variable determining the rate. In the flux-driven model, the system is nonisothermal and the exact temperature of

the reacting surface becomes virtually irrelevant once it reaches some threshold value. The traditional viewpoint, by contrast, focuses on that one intensive thermodynamic variable, T, and it does so only in one region of the system, the reaction zone. The newer viewpoint emphasizes extensive thermodynamic variables: The absorbing flux, I_{abs}, and the overall enthalpy change for the pyrolysis and devolatilization process, quite independent of the temperature of any one region of the nonisothermal system. In the newer model, the driving force for the reaction is the net energy flux density being absorbed by the reactant. The "barrier" to reaction is not some obscure activation energy, E_a, which must be overcome by raising the temperature of one particular region to a high enough level; rather it is the "resistance" or thermal inertia of the entire system that must be overcome. The thermal inertia is $\int_{T_o}^{T_s} C(T)\, dT + \Delta H_v$, and the reciprocal of that resistance is the "conductivity" of the reaction wave, which is its rate coefficient, k_t.

PYROLYSIS RATES AND STRUCTURAL MICROSCOPIC REALITIES FOR COAL

Kinetic data for the devolatilization rates of microscopic coal particles of varying diameter, heated in a CO_2 laser beam were reported previously (4, 5). The data at a constant input laser flux of 300 W/cm^2 for particles of 51-, 105-, and 310-μm average diameter are shown in Figure 2. The data show clearly that the time required for complete devolatilization increases monotonically with increasing particle diameter, as would be predicted by the flux-driven model of Figure 1. The effect of varying the incident laser flux for a given particle size was also studied.

For a more careful analysis of the data, it should be noted that the percentage mass loss versus time curves in Figure 2 have characteristic s-shapes. Since final volatility yields, $V(\infty)$, are approached only asymptotically as $t \to \infty$, it is most realistic to express the rate of the devolatilization reaction in terms of the time required for the particle to devolatilize to half its maximum value. That half life or $t_{1/2}$-value corresponds to the inflection point of the s-shaped curve. All the data are summarized in Figure 3, where the measured $t_{1/2}$ data points are plotted as a function of the incident laser flux for the three particle sizes studied. For the cubic particle with sides of width a_o, as depicted in Figure 1,

$$t_{1/2} = \frac{a_o}{2\dot{x}_o} = \frac{a_o\, \rho}{2k_t I_{abs}} \approx \frac{k' D_p}{(I - I_\ell')} \quad , \qquad 4)$$

where I_ℓ' is an effective loss flux and k' is a constant of proportionality which is linearly proportional to the thermal inertia of the devolatilization reaction, but which is also related to the shape of the particle and its orientation in the beam. The average particle diameter is D_p. The predictions of Equation 4 are also shown in Figure 3 as the dashed lines. The effective loss fluxes, I_ℓ', were taken as 50 W/cm^2 for the 51-μm particles, 25 W/cm^2 for the 105-μm particles, and 10 W/cm^2 for the 310-μm particles. These losses are mainly associated with conduction-convection to the cold surroundings, and their choice is discussed in detail elsewhere (5, 6). A constant k'-value of 1.46 kJ/cm^3 for all sizes gives the best fit to the data. The reasonable agreement between the data points and the theory curves predicted by Equation 4 tends to confirm the reasonableness of its derivation. It suggests that even on the microscopic level of particles as small as 50 μm, the pyrolysis process proceeds at a rate determined by the heat-transport-limited speed with which the devolatilization wave is driven through the particle by the heat source flux. The pyrolysis "rate constant" is determined by the thermodynamic properties of the medium, and no further assumption regarding a reaction kinetic mechanism appears to be necessary.

In terms of the actual thermal structure of the pyrolysis wave front, the data containing the most detailed spatial resolution were reported by Lee, Singer, and Chaiken (11) for large coal cylinders 1.8 cm in diameter and 5 cm high. Temperatures were measured every 3 mm. Their temperature profiles, obtained with the same laser but at much lower fire-level heat fluxes, are summarized in Figure 4.

They also obtained x-ray density profiles which showed that the reaction zone of active pyrolysis and devolatilization is characterized by a minimum density of 0.2 g/cm^3. These minimum density points are shown in Figure 4 superimposed on their measured temperature profiles. That reaction zone of minimum density is bounded on the cold side by unreacted coal (ρ = 1.33 g/cm^3) and on the hot side by a consolidated char residue (ρ = 0.85 g/cm^3). The reaction zone temperature corresponding to these minimum density points is 440-475° C.

The minimum density zone may be viewed as a "fizz zone" of active devolatilization composed of "frothing" liquid bitumen. The liquid bitumen consists of high-molecular-weight pyrolysis products, and it is frothing because lower molecular weight gases and tar vapors are bubbling through it. The bubbling "fizz zone" is also physically transporting the frothing mass of charifying liquid bitumen into the mass of previously formed char above it. The consolidated char of higher density is thus a compacted residue of the frothing mass of charifying liquid. Some secondary char-forming reactions are also occurring in the char layer above the fizz zone, as pyrolysis vapors diffuse through that cap of higher temperature char.

The data of Lee, Singer, and Chaiken also show clearly that the pyrolysis wave front propagates inward at a velocity that is proportional to the radiant flux; however, as the insulating char layer at the surface thickens in time, the surface temperature increases and flux losses to the cold surroundings increase markedly. It is not surprising, therefore, that the velocity of their pyrolysis wave front diminishes in time. Note also that the reaction zone temperature, however, remains essentially constant at 440-475° C, quite independent of the magnitude of the source flux that drives it, or the resultant velocity of the pyrolysis wave front. At their highest laser flux, the maximum temperature of the char layer at the surface was 760-800C. Because of the char layer expansion and swelling, the final surface is at a negative displacement relative to the original surface position at 0.0 cm.

That surface temperature may be considered to be the "source temperature" in such experiments since it is the char layer at the surface that directly absorbs the laser flux as time proceeds. Heat is then conducted through that char layer to the reaction zone below. Thus, although the source temperature is as high as 760-800° C for the higher flux data, the real temperature of the coal mass that is pyrolyzing and devolatilizing is only 440-475° C, and it would be incorrect to assign that char layer temperature to the reacting coal. It should also be noted that if the temperature of the coal sample or "particle" were measured optically from the surface spectral radiance, one would, of course, obtain only the surface temperature of the char residue and not the temperature of the reacting coal.

Structural data will now be presented that reveal the morphological changes in the coal structure that result from the propagation of such a pyrolysis wave front. The microscopic data will be presented for fine coal particles such as those used to obtain the data in Figures 2 and 3, and also for large coal samples comparable in size to those for which the data in Figure 4 were obtained. Scanning electron microscope (SEM) photographs of a coal particle exposed for 100 ms to a laser flux of 100 W/cm^2 are shown in Figure 5. The same particle is shown at two magnifications. The measured weight loss was only about 1 pct, and it can thus be inferred that the exposure time barely exceeded the induction time required for the surface of the particle to reach the decomposition temperature. There is, nevertheless, clear evidence that liquid bitumen was formed near the surface of the particle. That bitumen was oozing out from between the bedding planes while the particle was being heated, but after the beam was turned off, the surface cooled and the bitumen resolidified in the form of ridges. Those ridges are clearly seen to be oriented parallel to the bedding planes. A few blow holes are visible in those ridges of resolidified bitumen, but there are many more unbroken bubbles containing volatiles that were probably never emitted from the heated surface. Most of those volatiles have recondensed as liquid tars that are probably still contained within the bubble enclosures. Clearly, although devolatilization may have occurred within those bubbles, the process was not yet registered as a weight loss since the volatiles never broke through the bubble walls. The SEM photographs in Figure 5 suggest that the extent of thermal pyrolysis in a particle may be more extensive

than that obtained from the devolatilization weight loss. In order to be more precise, one should therefore distinguish between those two sequential processes. Pyrolysis or decomposition occurs first, and volatile emission occurs later. The photographs clearly illustrate the nature of the mass transport limitation involved in the transition between the generation of volatiles by thermochemical pyrolysis and their subsequent emission by bubble transport and rupture. It is only after the latter process is complete that a finite weight loss is registered.

The SEM photograph shown in Figure 6 is a later stage in the same process. It is a particle exposed for a time of 400 ms at a laser flux of about 125 W/cm^2. Based on its mass loss, the particle is somewhat more than half devolatilized, and it has clearly not reacted uniformly throughout its extent. Only the upper half of the particle (seen in Figure 6 as its right side) has devolatilized. The lower half of the particle (on the left) is essentially unreacted. It is the original coal structure. The laser beam was incident on the upper surface of the particle, and only the upper portion was devolatilized during the exposure time. It devolatilized into a dome or bubble, and after the volatiles contained within that dome were vented through blowholes, the whole structure seems to have started to collapse under its own weight. But, as it was collapsing, the higher molecular weight pyrolysis products that comprise the dome wall were simultaneously solidifying into a char. When they did solidify, a wrinkled skin residue was left.

The devolatilization wave thus appears to have traversed more than half way through the particle by the time the laser beam was turned off. The particle then cooled, and the devolatilization process was quenched with the pyrolysis wave "frozen" in place. Clearly the thickness of the wave front is substantially smaller than the particle diameter, and one can infer a wave front thickness of no more than 50 μm from the SEM photograph. Similar examples of such partially devolatilized particles are shown in Figure 7. Those particles are somewhat smaller in diameter and were exposed to a laser flux of about 100 W/cm^2 for about 1 s. Based on their average weight loss, the particles were about two-thirds devolatilized. In all four instances, the particles are viewed from the top, which was the surface on which the laser beam was incident. Blowholes and char residues are seen on the top portions of the particles. Unreacted coal residues with their cleaved edges and ledges are clearly visible at the bottoms of the particles. Again, the pyrolysis waves are frozen in place after having transversed only part of the way into the particles.

Experiments were also conducted with macroscopic coal samples of Pittsburgh seam bituminous coal, and those results are shown in Figure 8. The dimensions of the sample studied in Figure 8 and its orientation during laser exposure are sketched at the top of the figure. The face to be inspected by the SEM was deliberately cleaved some 20-30° beyond the vertical so that it would be "in the shadow" of the upper, irradiated surface. Exposure of the samples to a laser flux of 100-125 W/cm^2 for 2 s resulted in coking of the surface and its upward expansion as the char layer built up in thickness. Only the edge of the pyrolysis wave front moves down the cleaved face during that exposure time, and it is the edge that is viewed by the SEM, as illustrated in the sketch. The SEM photographs of the transition zone between the coal below and the char above are shown at three magnifications, with the largest magnification on the right. The transition region appears to be quite sharp. Despite the complications associated with the viewing angle, the swelling and frothing of the char layer, and the waviness of the pyrolysis front, one can estimate a reaction zone thickness for the quenched pyrolysis wave that is no larger than about 50 μm.

One must also realize that there is some thermal inertia in such a wave front so that its progression does not stop instantaneously after the laser source is turned off, especially if the wave front is being driven by the temperature gradient and thermal inertia of a char layer above it. The wave will inevitably progress to some extent during the decay time, and thermal diffusion during that same period may also thicken the wave front. The quenched "dead" wave seen in Figure 8 may therefore be somewhat broader than an active "live" wave. Such thermal inertia effects are even more significant for particles that are heated omnidirectionally in a furnace or a flow reactor than for the unidirectionally-heated particles described here.

A macroscopic sample of a Wyoming coal with a low-free swelling index (Hannah seam) was also studied by the same technique, and those results are reproduced in Figure 9. There was substantial cracking of the sample caused by the mechanical stresses induced by the high temperature gradient laser exposure (100-125 W/cm^2 for 2 seconds). Those fractures provide a revealing, three-dimensional view of the structure of the transition zone between the char above and the coal below. The position of the pyrolysis wave front is indicated in Figures 9A-F by the arrows at the edges of the SEM photographs. A detailed analysis of the structure is given elsewhere (6), but again the data give an intrinsic width of the wave front that is less than 50 μm.

These SEM photographs in Figures 5, 6, 7, 8, and 9 clearly reveal the existence of the pyrolysis wave front and its structural reality on the microscopic scale. They strongly support the newer viewpoint that the process occurs in the form of the inward progression of a pyrolysis wave front from the exposed surface. Even for small particles, these microscopic realities directly contradict the traditional viewpoint that the reaction process occurs isothermally throughout the particle.

PYROLYSIS AND DEVOLATILIZATION OF PMMA

Long cylinders of polymethylmethacrylate (PMMA) with diameters of 0.45 cm were oriented on end, and exposed to the same CO_2 laser beam. The pyrolyzing upper surface of the rod maintained its circular cross section as the surface regressed downward along the axis of the cylinder. The weight or mass loss per unit area, Δm, was measured as a function of exposure time in a given laser flux. The data are summarized in Figure 10. The good linearity of the Δm versus time curves indicate that steady-state conditions were obtained. Lines are drawn in Figure 10 for the least squares fits to the data points at each flux level. The lines are well represented by the equation

$$\Delta m = \dot{m} (t - \tau). \qquad 5)$$

The slope of each line thus represents the steady-state devolatilization rate, $\dot{m}$, at each flux, and the horizontal intercept is the induction time, τ, at that flux. Clearly, the induction time is simply the time required for the surface of the sample to be heated to the devolatilization temperature. The steady-state rates are plotted in Figure 11 as a function of the net incident flux $I(1 - r) = 0.93\ I$, where the reflectance, r, is taken as 7 pct. A least squares fit to the five sets of data points in Figure 11 gives

$$\dot{m}\ (mg/cm^2 s) = 0.72\ (mg/J)\ [0.93\ I - 9.8]\ (W/cm^2). \qquad 6)$$

The inferred steady-state loss flux is therefore $I_\ell = 9.8$ W/cm^2, and the rate coefficient for the pyrolysis and devolatilization of PMMA is therefore k_t (PMMA) = 0.72 mg/J = 3.01 g/kcal. Its reciprocal, $1/k_t = 332$ cal/g, is the thermal inertia of the pyrolysis wave. According to Equation 3, the thermal inertia is given by $\int_{T_o}^{T_s} C(T)dT + \Delta H_v$. Taking the decomposition temperature for PMMA as 400 °C (12), the heat capacity data reported by Bares and Wunderlich (13) give $\int_{25}^{400} C(T)\ dT = 196$ cal/g. The calorimetrically measured value for the heat of depolymerization of PMMA (corrected to 400° C) is 126 cal/g (14). The sum, 322 cal/g, is therefore the calculated thermal inertia of the system. The thermodynamically predicted rate constant obtained from Equation 3 for the pyrolysis and devolatilization of PMMA is thus in excellent agreement with the measured value obtained from Figure 11. Furthermore, the measured slope from Figure 11 for data obtained at radiant fluxes of 12-115 W/cm^2 is in quite good agreement with the slopes measured independently by Vovelle, Akrich, and Delfau (15) and by Kashiwagi and Ohlemiller (12). Their data were obtained at radiant fluxes in a much lower range of 1.4-4.0 W/cm^2. A detailed analysis of both their data is presented elsewhere (6). Their data were for vertically oriented slabs of PMMA with much larger cross-sectional areas of 10 x 10 cm^2 and 4 x 4 cm^2, respectively. Accordingly, their loss fluxes were only about 1.0 and 1.5 W/cm^2, respectively, but their plotted slopes were essentially the same as those in Figure 11.

The coal data presented earlier can also be used to obtain estimates for the coal's k_t-value. The macroscopic $\dot{m}$ versus I curves reported by Lee, Singer, and Chaiken (11) have also been analyzed in detail elsewhere (6), and their measured slope gives k_t = 0.75 g/kcal for coal. The microscopic particle data shown in Figure 3 can also be used to infer a rate coefficient for coal of $k_t = \rho/2k' =$ 1.91 g/kcal, which is a factor of 2-3 higher. Clearly those data for coal are substantially less accurate than the PMMA data. A difference of a factor of 2 or 3 for independently-measured rate coefficients for coal is probably the best one can expect considering the complexities associated with the coal's insulating char layer, the uncertainties in the shape factors for the fine particles, the in-depth absorption of the laser beam which is significant for particle dimensions but trivial for large samples, the two orders of magnitude range in incident fluxes, and the three orders of magnitude differences in sample size. Thus there is considerable uncertainty in the k_t-value for coal, but the available data suggest that it is somewhat lower than the value for PMMA. Clearly, except for the complication of the coal's char layer residue and its more complex devolatilization thermodynamics, there appear to be no other extraordinary differences in the pyrolysis and devolatilization behavior for the two substances. Both pyrolysis rates are describable in terms of the progression of a decomposition wave whose speed of propagation is controlled by thermodynamic transport constraints.

Returning to the PMMA data, Kashiwagi and Ohlemiller (12) and Kashiwagi (16), also measured surface temperatures during devolatilization, and those data are shown in Figure 12. Their data, obtained at two flux levels show that $\dot{m}$-values are insignificant until some threshold temperature is approached, at which point the rate becomes exceedingly rapid as the $\dot{m}$ versus T curve turns vertically upward. Above the threshold temperature, the rate of pyrolysis and devolatilization becomes virtually insensitive to the surface temperature. For the exposed surface to reach the decomposition temperature of 350-400° C, a minimum threshold heating flux is required in order to overcome the loss flux, I_ℓ. A theory curve is shown in Figure 12 which is a simple step function at T_s, and it represents the assumption implicit in the derivation of Equations 2 and 3.

According to the assumption used for the new model, there is no devolatilization in the horizontal portion of the curve ($\dot{m} = 0$) until the surface temperature of the sample reaches the decomposition temperature, T_s. Once the surface reaches the decomposition temperature T_s, the rate becomes finite and one is in the vertical portion of the step function. The rate is then controlled entirely by the source flux intensity, and the temperature of the reacting surface becomes both invariant and virtually irrelevant.

The model represented by Equations 2 and 3 thus uses a step function to approximate the finite curvature of the transition depicted in Figure 12. In the horizontal portion of the step, the surface is heating up in the input flux, but there is no devolatilization occurring because the temperature is too low. Once the temperature reaches T_s and significant pyrolysis and devolatilization begin, one transits into the vertical portion of the step, and the system is under heat transport control.

It is also interesting to compare the measured induction times for the onset of the pyrolysis and devolatilization process for the PMMA samples with those predicted on the basis of the measured T_s value of 400° C and the exact solution to the time-dependent heat transport equation. For a semi-infinite solid whose surface is heated by a constant source flux, Carslaw and Jaeger (17) give:

$$\tau = \frac{\pi}{4} C \rho \lambda (T_s - T_o)^2/[I(1-r)-I_\ell]^2. \qquad 7)$$

The time required for the surface to reach the temperature T_s is the induction time, τ. The system is initially isothermal at T_o = 25° C. The heat capacity, C, is taken as the average value for the temperature range between T_o and T_s, which is 0.52 cal/g °C (13). The density ρ is 1.18 g/cm^3, and the thermal conductivity λ is taken as 4.5 x 10^{-4} cal/cm s °C (14). The source flux is taken as $I_{abs} = I(1-r)-I_\ell$.

The comparison between the measured τ-values from Figure 10 and those calculated from Equation 7 is shown in Table 1. The comparison is made for two cases: one with the measured steady state loss flux of $I_\ell = 9.8$ W/cm^2; the other for $I_\ell = 0$. Initially at $t = 0$, the entire sample is at ambient temperature and $I_\ell = 0$; however, as $t \to \tau$, $I_\ell \to 9.8$ W/cm^2. Clearly during the non-steady-state induction period as the surface temperature increases from $T_o = 25°$ C to $T_s = 400°$ C, the loss flux, which is due mainly to conduction and convection to the cold surroundings, increases from 0 to 9.8 W/cm^2. The loss flux is clearly time-dependent, but its average value should vary between those two limiting cases. The table clearly shows that the measured τ-values fall between the two predicted limiting cases. The only exception is the measured τ-value at the highest flux which is about a factor of two higher than the calculated value. That difference is attributed to the finite absorption depth of the laser beam. At low fluxes that absorption depth is trivial compared to the characteristic width of the subsurface temperature profile; however, at the highest flux, the two may be of comparable dimensions. Such in-depth absorption is significant at the the highest flux, and a larger mass near the surface is actually heated by the flux than is calculated from the simple theory from which Equation 7 was derived. As a result, the actual induction time required for the surface to reach T_s for in-depth absorption is longer than that calculated on the assumption that the flux is deposited entirely at the surface.

Table 1. - Comparison of Measured Induction Times for the Laser Pyrolysis of PMMA with Theoretical Calculations of Equation 7

Laser Flux, W/cm^2		Induction Time, τ, s		
Incident	Net		Calculated, Equation 7	
I	$I_{abs}=I(1-r)-I_\ell$	Measured	$I_\ell = 9.8$ W/cm^2	$I_\ell = 0$
115.0	97.2	0.101	0.057	0.047
71.0	56.2	0.160	0.169	0.123
42.5	29.7	0.50	0.605	0.342
23.2	11.8	1.83	3.84	1.16
12.4	1.73	6.70	178	4.04

It should also be noted that the theory curves in Figure 3 for coal particles are based on the steady state condition and are uncorrected for such induction time delays. At the higher fluxes, especially for the larger particles, the τ-corrections are small in comparison to the steady-state $t_{1/2}$-values. The corrections are however significant at the lower fluxes for the smaller particles. Nevertheless, there is also a decay time correction required, as discussed earlier. The pyrolysis wave's thermal inertia results in some continuing propagation even after the source flux is turned off. These non-steady-state corrections for induction time and decay time would tend to counteract one another.

PYROLYSIS AND DEVOLATILIZATION IN DUST FLAME PROPAGATION

The flame propagation processes in pulverized coal-fired burners or in accidental dust explosions (18) are examples of combustion processes in which the pyrolysis and devolatilization of the solid fuel particles play a key role. Flame propagation in dust-air mixtures involves three sequential processes (19): heating and devolatilization of the dispersed dust particles; mixing of the emitted volatiles with air in the space between particles; and gas phase combustion of the premixed fuel-air mixture. Each sequential process has its characteristic time constant: τ_{dv}, τ_{mx}, and τ_{pm}. The resultant burning velocity of the dust-air flame, S_u, will be given by $S_u = (\alpha/\tau_e)^{1/2}$ where α is the effective diffusivity for heat and/or free radical mass transfer across the flame front, and τ_e is the effective time constant for the completion of the above sequence of processes. The slowest of those processes will be the rate-limiting process, and accordingly, the resultant τ_e will be controlled by the slowest of those τ-values.

For very fine dust particles at low, lean-limit concentrations, the first two processes are so rapid that the propagation rate is controlled by the last process:

gas-phase combustion. Since that is essentially the same process that controls homogeneous, premixed, gaseous flames, dust flame behavior in those limits is virtually identical to that of an equivalent homogeneous gas-air mixture of the dust's volatiles (20, 21). Thus for very fine dust particles at lean-limit concentrations, each particle is completely devolatilized within the flame front, and the lean limit concentration of the dust-air mixture is determined by the total combustible volatile content of the dust. For example, the lean-limit mass concentration for fine polyethylene, CH_3-$(CH_2)_n$-CH_3, a dust that devolatilizes completely in its lean-limit flame, is identical to that of homogeneous gas-air mixtures of the saturated alkanes (20, 21).

For homogeneous gas flames, there exists a minimum burning velocity for natural convective quenching of about 3 cm/s, below which normal flame propagation is impossible (22, 23). For dust flames, the limit burning velocity appears to be somewhat higher for a variety of reasons (24). For a homogeneous gas flame of burning velocity S_u, the characteristic width of the flame front is $\delta=\alpha/S_u$ and the characteristic time for the completion of the homogeneous gas phase reactions is $\tau_{pm} = \delta/S_u = \alpha/S_u^2$. Setting $\alpha = 0.55$ cm/s and $S_u = 3$ cm/s for the limit burning velocity gives $\tau_{pm} = 60$ ms. That 60 ms is the characteristic time required for the completion of the gas-phase reactions, and if the rate processes are slower than that, the normal high-temperature flame propagation process is quenched by natural convection (23). For heterogeneous dust-air flames the situation appears to be somewhat more complicated. The limit velocities appear to be about a factor of 2 higher, but at the same time the flame zone thicknesses appear to be broader (24). A higher S_u would, for homogeneous flames, normally be associated with thinner flame fronts according to the previous equation, $\delta= \alpha/S_u$. A higher burning velocity and a thicker flame front for dusts suggest that the dust flame is always somewhat accelerated by turbulent vortices which enhance the diffusivity factor, α, increasing it to a value that is higher than the normal laminar one (24). Those vortices are associated with the dust fuel concentration, which is intrinsically inhomogeneous on the scale of either the particle diameter or the distance between particles. In any case, that complication for dust flames leaves one with an uncertainty in the proper choice for τ_e for the heterogeneous flame. It will be here assumed that for heterogeneous flames, the higher S_u at the limit and the wider flame zone thickness (24) give a τ_e that is about a factor of 2 longer than for homogeneous flames, so that 120 ms is chosen for τ_e. That value is thus the maximum time available for pyrolysis and devolatilization. If the process takes any longer, the volatiles are emitted in the burned gases, which is too late for them to contribute to the propagation process within the flame front.

As dust concentrations increase above their lean limit values, or as the dust particles become coarser, the heating and devolatilization process will begin to become rate limiting. In the former case, as stoichiometric concentrations (with respect to the volatiles) are approached, S_u for hydrocarbon-like dusts approaches its maximum value of about 40 cm/s (25). Since τ_e varies as $(S_u)^{-2}$, that order of magnitude increase in S_u reduces τ_e by two orders of magnitude: from 120 ms to only about 1 ms. For such rapidly propagating dust flames, only the surface regions of the dust particles can contribute volatiles to the flame. The flame "rides the crest" of a near-stoichiometric concentration of volatiles regardless of the initial dust loading. That devolatilization rate limitation is responsible for the absence of a "normal" rich limit of flammability for dusts. Although excess fuel volatiles may continue to be emitted in the burned gases at high dust loadings, they are emitted too late to dilute the flame front with excess fuel vapor (18, 20, 21).

Data for the particle size dependence of the lean limits of flammability for coal and PMMA, as measured in a 20-L chamber (26), are shown in Figure 13. They show clearly how the pyrolysis and devolatilization rate process becomes rate limiting as the dust particles become coarser. The curves for coal and PMMA have similar shapes. The initially flat region demonstrates a lean limit that is independent of particle size as long as the particle diameter is small enough. The smaller particles can all totally devolatilize in the time available, and the system behaves as an equivalent homogeneous premixed gas. As diameters increase, the

curves turn upward at some characteristic diameter because of the devolatilization rate limitation, and a size dependence begins to appear. As shown earlier in Figures 2 and 3, for a given heating flux the devolatilization time increases linearly with particle diameter. Thus the pyrolysis and devolatilization rate limitation appears to adequately explain the shapes of the curves. For a fixed flame flux, the time required for devolatilization τ_{dv} will vary linearly with the particle diameter D_p. Below some characteristic diameter, $\tau_{dv} << \tau_{pm}$, the particles can devolatilize completely in the time available, and τ_e is controlled by the gas phase combustion reactions. In that range of fine particle sizes there is no size dependence. However, as $\tau_{dv} \rightarrow \tau_{pm}$, the devolatilization rate process becomes significant in the overall flame propagation process and a particle size dependence begins to appear. For still coarser sizes, $\tau_{dv} >> \tau_{pm}$, and the rate of devolatilization becomes rate controlling. Only the surface regions of the coarser dust particles can then devolatilize in the 120 ms that is available for flame propagation, and hence, a higher dust loading is required to generate a lean limit concentration of combustible volatiles. The curves must therefore turn upward. Eventually, when the particles are so coarse that an excessive dust loading is required, then other thermal quenching processes become significant, and the critical diameter is reached above which propagation is impossible even at the highest dust concentrations. Those critical diameters are the vertical asymptotes of the curves in Figure 13.

A more quantitative analysis is possible using the pyrolysis and devolatilization rate constants reported here for coal and PMMA. The coal value was uncertain by a large factor, but it was nevertheless lower than the k_t-value for PMMA, which was 3.01 g/kcal. According to Equation 3, when exposed for a time t to a net flux I_{abs}, a devolatilization wave front will travel a distance $x = \dot{x}_o t = k_t I_{abs} t/\rho$. For dust flames at their limits of flammability, the I_{abs} and t values are comparable for the two dusts. For PMMA, the rate constant is higher than for coal, and its density is only slightly lower. Thus, Equation 3 predicts that the characteristic diameter for PMMA should be somewhat larger than the value for coal. The data curves in Figure 13 support that expectation.

A prediction of the absolute magnitude of the characteristic diameter is also possible. As indicated earlier, the time available for devolatilization within a heterogeneous flame front propagating at the limit velocity is t = 120 ms. But what value is one to use for I_{abs} when the particle is being heated in a flame front? The major uncertainty in predicting the characteristic diameter is the uncertainty in estimating, I_{abs}, the effective or net heating flux to which the particles are exposed as they approach, enter, and traverse through the flame front. For homogeneous gas flames, radiation from the burned gases to the unburned fuel is usually not significant because the unburned gaseous mixture has a trivial absorptivity. That is not the case for dust particles, so that well before the particles actually enter the flame front, they will absorb the radiance emitted from the hot combustion products, which consist of burned gases, soot, and char. Typically, hydrocarbon flames exhibit a fairly constant limit flame temperature of 1400 to 1500 K, and the Planck radiance at those temperatures is 5-7 cal/cm^{2}s. But for a spherical particle approaching a flame front, that radiance is seen only by its forward-facing hemisphere. That radiance will however be seen for a considerably longer time period than the particle's 120-ms residence time in the flame front. As the particle heats up in that radiance, it will, however, lose an increasing fraction of that radiance by conduction and convection to the surrounding cold air. It is difficult to estimate the effects of that radiant heat transport process, but it is clear from the previous estimate of the particle loss fluxes, which were as high as 50 W/cm^2 for 50-μm particles at T_s = 450-600° C, that the particle temperatures will remain well below the decomposition temperature during that approach period. The particle could nevertheless be preheated significantly above ambient temperature as it enters the flame front. Upon entering the flame front, there is an additional conductive-convective heat flux from the hot gases within the flame front. That heating flux increases in magnitude as the particle penetrates into the burned gases. As it begins to devolatilize in that

conductive-convective flux, the heat transport process becomes exceedingly complex, and the "blowing effect" of the emitted volatiles markedly reduces the Nusselt number. Realistic estimates are difficult to make; however, in (25) it is estimated that the average power density across a homogeneous, laminar, flame-front is given by S_u C ρ (T_b-T_u). For the dust flames under limit conditions S_u = 6 cm/s, C = 0.35 cal/g K, ρ=1.5 x 10^{-3} g/cm^3, and T_b-T_u = 1500-300 = 1200 K. The resultant is an average conductive-convective flux of about 4 cal/cm^2s. If one adds to that flux about half of the previously estimated radiant flux (since only the forward hemisphere of the particle sees the flame), one obtains I_{abs} = 7 cal/cm^2s. For PMMA, the travel distance of the devolatilization wave into the particle during its exposure within the flame front thus becomes $x = k_t I_{abs} \tau_e/\rho$ = 21 μm. Thus for PMMA the depth of penetration of the devolatilization wave front in the time available for flame front passage under near limit-conditions is about 21 μm. For a square particle heated from two opposing faces, the predicted characteristic diameter would therefore be $\overline{42}$ μm. For a spherical particle in an omnidirectional source flux, the devolatilization of an outer shell 21-μm in depth would actually represent the devolatilization of some 90 pct of the mass of a 75-μm-diameter particle. One should also realize that such omnidirectional heating generates a converging wave front which will accelerate as heat accumulates within the particle. Equation 3 was derived for a planar, steady-state wave front. The converging wave will penetrate farther into the particle during the same exposure time. Accordingly, one estimates that the measured rate coefficient for PMMA should correspond to a characteristic diameter of about 80-100 μm for spherical particles. That estimate is also in fair agreement with the data in Figure 13.

CONCLUSIONS

On the basis of a detailed analysis and evaluation of a diverse set of experimental observations reported by many independent investigators, and on the basis of the data reported here for pyrolysis rates and microscopic structure, it is concluded that there is no substantive evidence to support the traditional viewpoint that the coal particle pyrolysis process proceeds isothermally, under chemical rate control, or that it is describable by a unimolecular, Arrhenius function of the source temperature, T_h, to which the coal particles are exposed. The overwhelming weight of evidence shows that the process occurs in the form of a non-isothermal decomposition wave whose propagation velocity is linearly proportional to the net absorbed heat flux intensity and inversely proportional to the overall enthalpy change for the reaction.

The pyrolysis and devolatilization "rate coefficient" is the reciprocal of that overall enthalpy requirement for heating and devolatilization. Although the rate coefficient for Pittsburgh seam bituminous coal is smaller than that for the simple polymer, PMMA, the pyrolysis and devolatilization behavior of the coal is not markedly different from that of PMMA, except for the complications associated with the coal's char layer residue.

At fire and burner level heat fluxes of 10-100 W/cm^2 and above, the pyrolysis and devolatilization behavior of coals and polymers is realistically describable by the thermodynamic transport-controlled model in which the intrinsic rate of decomposition is described as a simple step-function at the decomposition temperature, T_s. Below T_s the intrinsic rate is near zero. At T_s, the intrinsic rate is so rapid that the system is heat transport controlled. There is no substantive evidence that the temperature of the reactant during pyrolysis and devolatilization can significantly exceed T_s, regardless of the source temperature, T_h, to which it is exposed. For PMMA, T_s is 350-400 °C; for the coal it is 450-600 °C.

REFERENCES

1. Van Krevelen, D.W. Coal Typology-Chemistry-Physics-Constitution, Elsevier, 1961, 514 pp.
2. Badsiock S. and P. G. W. Hawksley. Industrial Engineering Chemistry, Process Des. Develop. 9 (1970), p. 521
3. Anthony, D. B. and J. B. Howard. AIChE Journal, 22 (1976), p 625.
4. Ng, D. L., M. Hertzberg, and J. C. Edwards. A Microscopic and Kinetic Study of Coal Particle Devolatilization in a Laser Beam. Poster Session Paper No. 83, 20th Combustion Symposium, 1984.
5. Hertzberg, M. and D. L. Ng. NATO Advanced Research Workshop on Fundamentals of Physical Chemistry of Coal Combustion, ed. by J. Lahaye, NATO Series Catalogue, Martinus Nijhoff, to be published 1987.
6. Hertzberg, M., I. A. Zlochower, and J. C. Edwards. Coal Particle Pyrolysis Mechanisms and Temperatures. Bureau of Mines Report of Investigation, to be published 1987.
7. Zielinski, E. Fuel 46 (1967), p 329.
8. Freihaut, J. D. and F. J. Vastola. Eastern Section - Combustion Institute, Fall Technical Mtg., Miami Beach, Florida, Nov. 29-Dec. 1, 1978, p 32-1.
9. Solomon, P. R., R. M. Corangelo, P. E. Best, J. R. Markham, and D. G. Hamblen. The Spectral Emittance of Pulverized Coals and Char. 21st Symposium (Int.) on Combustion, to be published 1987.
10. Solomon, P. R., and M. A. Serio. Evaluation of Coal Pyrolysis Kinetics. NATO Advanced Research Workshop on Fundamentals of Physical Chemistry of Coal Combustion, ed. by J. Lahaye, NATO Series Catalogue, Martinus Nijhoff, to be published 1987.
11. Lee, C. K., J. M. Singer, and R. Chaiken. Comb. Sci. and Techn., 16 (1977), p 205.
12. Kashiwagi, T. and T. J. Ohlemiller. 19th Symposium (Int.) on Combustion, Combustion Institute, 1982, p 815.
13. Bares, V. and B. Wunderlich. J. Polymer Sci, Polymer Phys Edition, 11 (1973), p 861.
14. Brandrup, J. and E. H. Immergut. Polymer Handbook, 2nd ed, J. Wiley and Sons (1975), pp II-425 and V-56.
15. Vovelle, C. R. Akrich, and J. L. Delfau. Comb. Sci. and Techn., 36 (1984), p 1.
16. Kashiwagi, T. Combustion and Flame, 34 (1979), p 231.
17. Carslaw, H. S. and J. C. Jaeger. Conduction of Heat in Solids, 2nd ed., Oxford, p 75.
18. Hertzberg, M. and K. L. Cashdollar. Introduction to Dust Explosions, in STP 958, Industrial Dust Explosions, American Society for Testing and Materials, Philadelphia, PA 1987, to be published.
19. Hertzberg, M., K. L. Cashdollar, D. L. Ng, and R. S. Conti. 19th Symposium (Int.) on Combustion, Combustion Institute, 1982, p 1169.
20. Hertzberg, M., K. L. Cashdollar, and I. A. Zlochower. Flammability Limit Measurements for Dusts and Gases: Ignition Energy Requirements and Pressure Dependencies, 21st Symposium (Int.) on Combustion, Combustion Institute, to be published 1987.
21. Hertzberg, M., I. A. Zlochower, and K. L. Cashdollar. Volatility Model for Coal Dust Flame Propagation and Extinguishment, 21st Symposium (Int.) on Combustion, Combustion Institute, to be published, 1987.
22. Hertzberg, M. Bureau of Mines RI 8127, (1976).
23. Hertzberg, M. 20th Symposium (Int.) on Combustion, Combustion Institute (1984), p 1967.
24. Klemens R. and P. Wolanski. Flame Structure in Dust and Hybrid Mixtures Near the Lean Flammability Limit. Poster Session Paper No. 100, 20th Combustion Symposium, 1984.
25. Hertzberg, M. Bureau of Mines RI 8469, (1980).
26. Cashdollar, K. L. and M. Hertzberg, Rev. Sci Instrum., 56 (1985) p. 596.

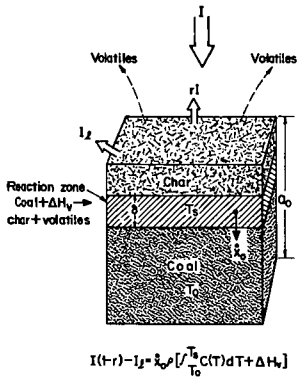

Figure 1. - A schematic idealization of the propagation of a planar steady-state pyrolysis and devolatilization wave front in coal as it is being driven by a plane-wave radiant source flux of intensity, I.

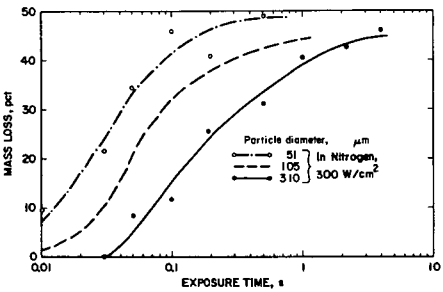

Figure 2. - The devolatilization mass loss for coal particles of 51, 105, and 310μm diameter as a function of exposure time at a constant laser source intensity of 300 W/cm^2, from reference 5.

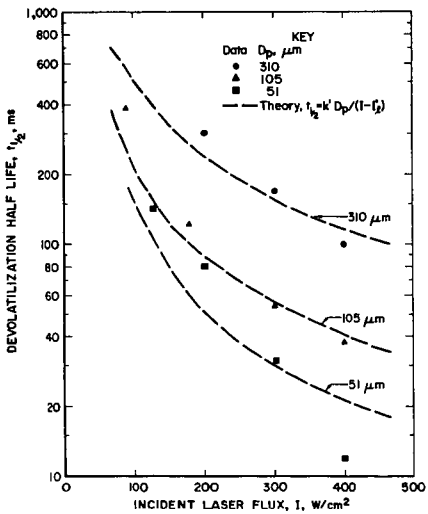

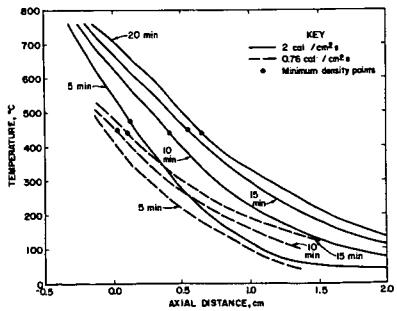

Figure 4. - Measured temperature profiles for coal during pyrolysis and devolatilization as a function of time for two laser intensities, as measured by Lee, Singer, and Chaiken(11).

Figure 3. - Summary of the measured half lives for coal particles as a function of laser source intensity for the three coal particle sizes from reference 5. The data points are compared with the theory based on heat transport limitations according to the First Law of Thermodynamics.

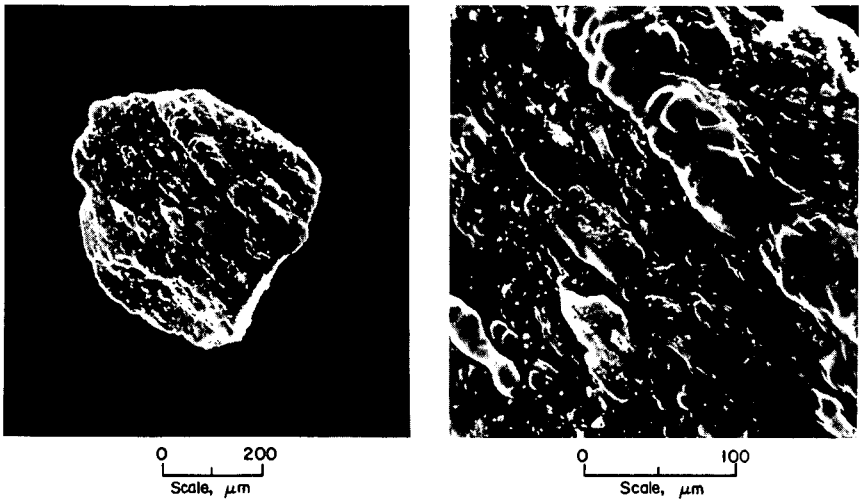

Figure 5. - Scanning Electron Microscope (SEM) photographs of the exposed surface of a coal particle exposed for 100 ms to a laser flux of about 100 W/cm^2, seen at two magnifications.

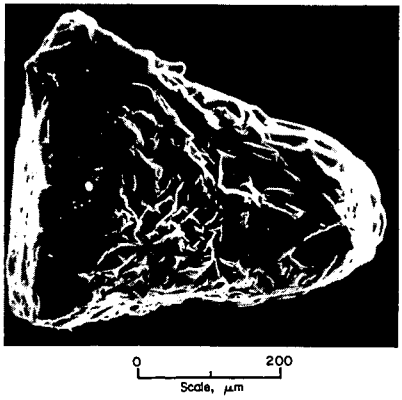

Figure 6. - SEM photograph of a coal particle, which is about two-thirds devolatilized after exposure for 400 ms to a laser flux of about 125 W/cm^2.

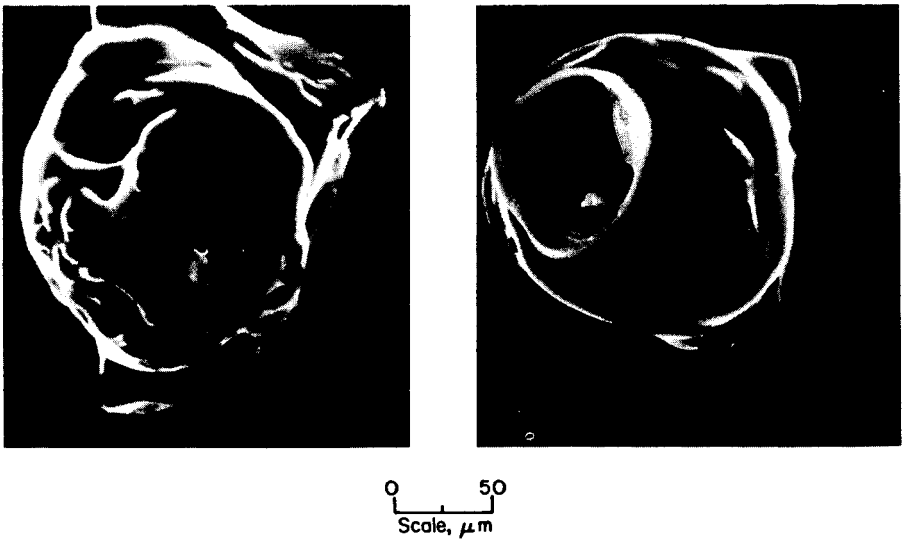

Figure 7. - SEM photographs of four different particles exposed to a laser flux of about 100 W/cm^2 for 1 s. The particles are all about two-thirds devolatilized by the laser flux incident from above.

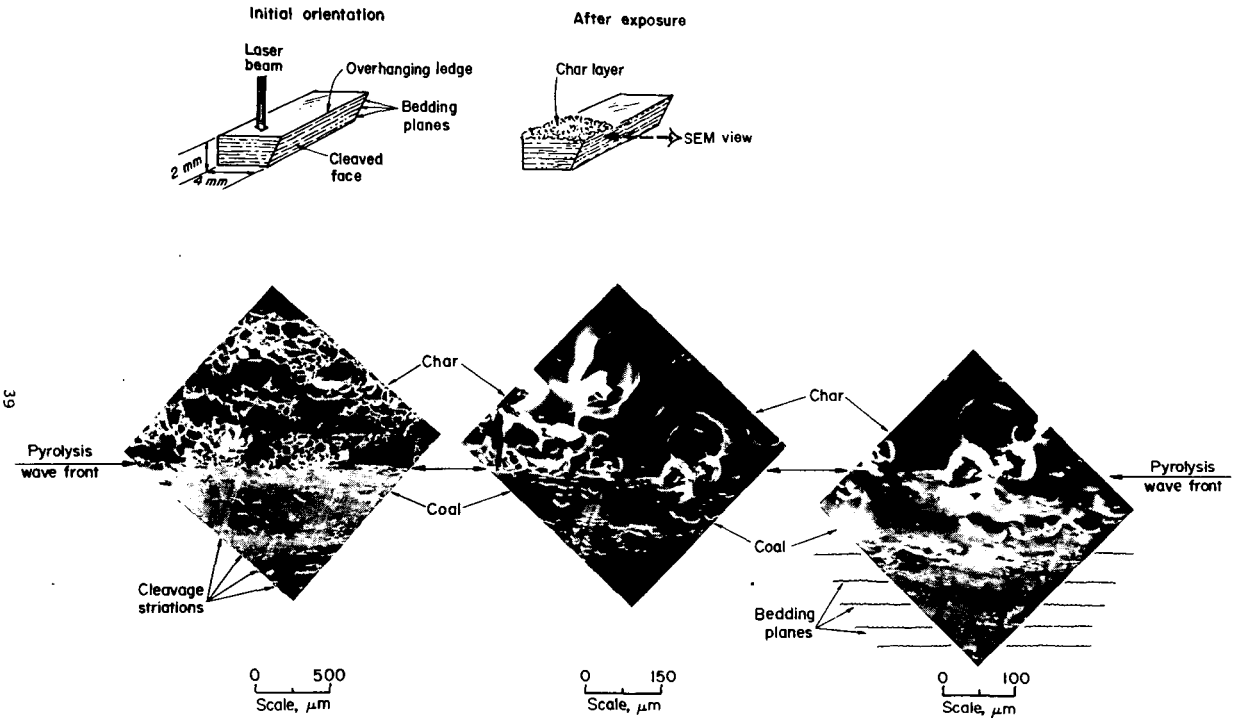

Figure 8. - SEM photographs viewed from the side of a shadowed, cleaved face of a macroscopic sample of Pittsburgh seam bituminous coal exposed for 2 s to a laser flux of 100-125 W/cm^3. The pyrolysis and devolatilization wave front is viewed at three magnifications.

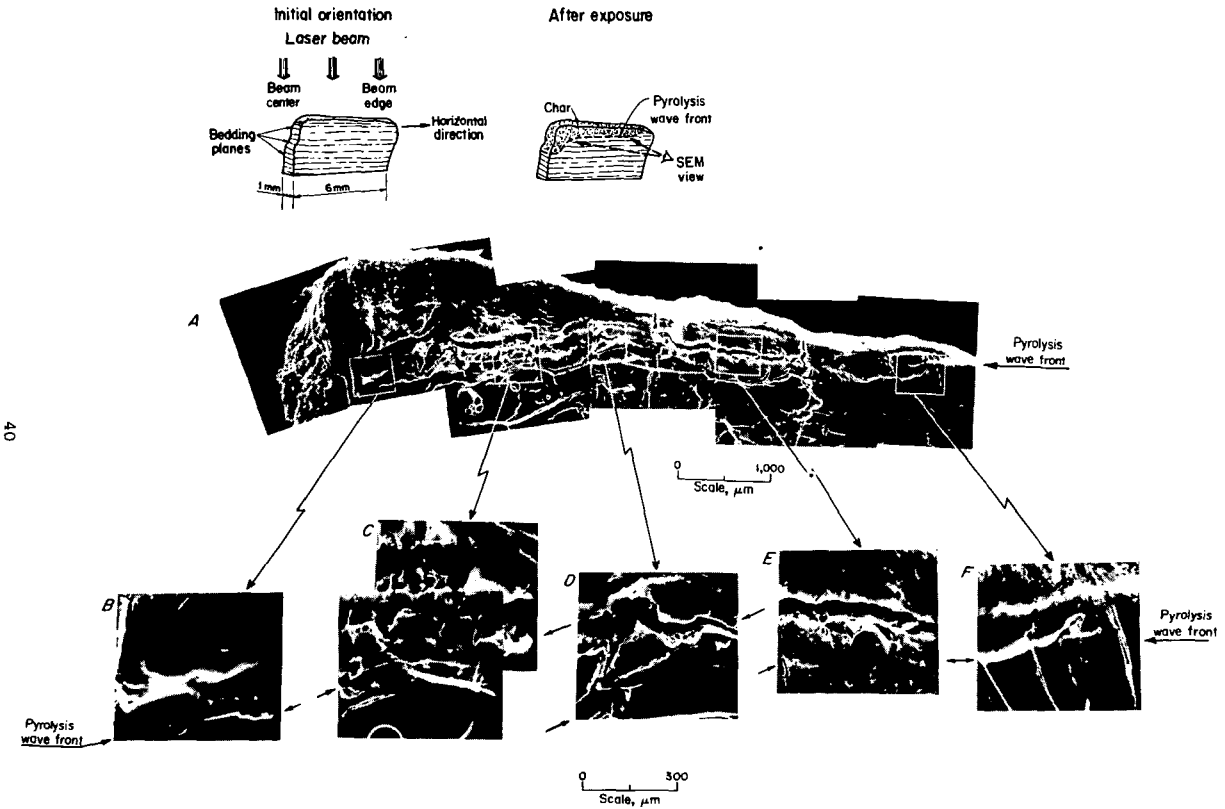

Figure 9. - SEM photographs of a macroscopic sample of the Hannah-seam coal exposed to a maximum laser flux of 100-125 W/cm^2 for 2 s, as viewed from the side. Lower magnification montage in A; higher magnification views of the pyrolysis and devolatilization wave front in B, C, D, E, and F.

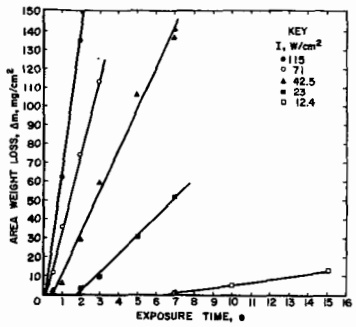

Figure 10. - The measured pyrolysis and devolatilization weight (or mass) losses for 0.45 cm diameter, PMMA cylinders as a function of exposure time for different input laser flux intensities in the range 12 to 115 W/cm^2.

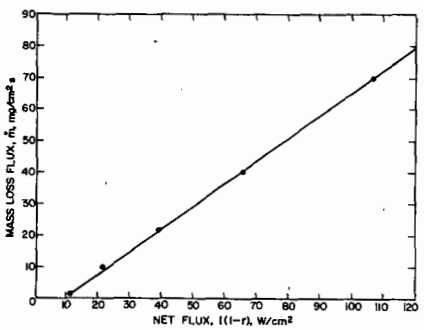

Figure 11. - The measured, steady-state rates of pyrolysis and devolatilization for 0.45 cm diameter PMMA cylinders, as a function of input laser flux corrected for surface reflectance, r.

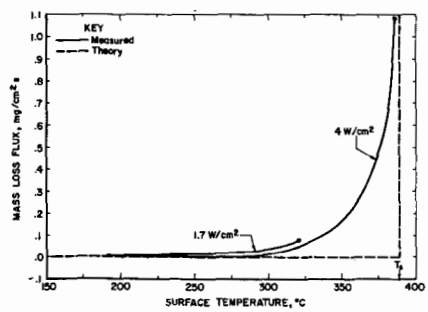

Figure 12. - The measured surface temperatures at various mass loss rates during the pyrolysis and devolatilization of PMMA at two radiant fluxes as reported by Kashiwagi and Ohlemiller. Measured values compared with simplified, step-function theory using a discrete, decomposition temperature, T_s.

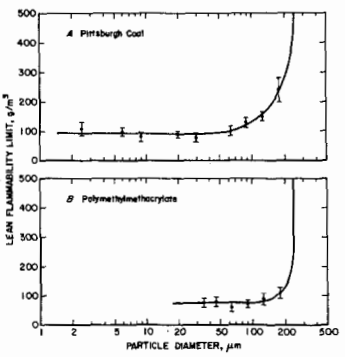

Figure 13. - Lean flammability limit as a function of particle diameter for Pittsburgh seam bituminous coal and polymethacrylate.

SPECTRAL EMISSION CHARACTERISTICS OF SIZE-GRADED COAL PARTICLES*

Thomas H. Fletcher, Larry L. Baxter and David K. Ottesen

Sandia National Laboratories, Livermore, CA 94550

The spectral emission characteristics of coal are examined using Fourier transform infrared emission spectroscopy. The data were collected from a single layer of stationary, narrowly size-classified samples of coal and graphite placed on a heated NaCl window. Sample temperatures ranged from 120 to 200°C. FTIR data were collected at wavelengths between 2.2 and 17 μm (between 4500 and 580 cm^{-1}). Particle sizes ranged from 40 to 120 μm and coal rank ranged from lignite to bituminous.

The focus of this work is to evaluate the effects of the nongray emission characteristics of coal on heat transfer calculations and pyrometry measurements. Chemical functional groups responsible for the features of the spectral emission are identified but not discussed. Well characterized spectral features from coal samples are observed and discussed. The intensity of spectral peaks due to chemical functional groups in coal are analyzed as a function of particle size and extent of reaction. The impact of spectral irregularities on pyrometry measurements and heat transfer calculations is evaluated. Featureless regions of the infrared emission spectra of coal are also analyzed and compared to graybody behavior. Reliability of pyrometry measurements in these regions and effective emissivities of coal particles for heat transfer calculations are discussed.

INTRODUCTION

Spectral and total emission characteristics of coal have been reported in the past, with emissivities ranging from 0.1 to near unity. Several investigators (1-3) have published results indicating that coal is not a strong absorber of radiation at infrared wavelengths. Values of the imaginary part of the complex index of refraction on the order of 0.05 are reported by these authors. Other authors report much larger imaginary coefficients, of the order of 0.3 (4-6), indicative of higher abosrbance and emittance of radiation.

A strong and irregular dependence of emissivity on wavelength would be expected of an organic compound containing a variety of chemical functional groups, such as coal, if the material is either generally transparent or very thin. Such results are reported by Solomon and coworkers (3) for particles less than 40 μm in diameter, although the size of the particles is not always well defined in their work. Commonly available infrared absorption and diffuse reflectance spectra of coal samples are consistent with the spectral features reported by Solomon. However, these features should become indistinguishable from the diffuse background absorption as the particle size increases. Solomon noted this trend, but did not define a particle size where the spectral features of the emission become insignificant compared to the diffuse background radiation. Large or highly absorbing particles should show less variation of emissivity with wavelength; they should become approximate gray-bodies.

* Research conducted at the Combustion Research Facility, Sandia National Laboratories, Livermore, California, and sponsored by the U.S. Department of Energy through the Pittsburgh Energy Technology Center's Direct Utilization Advanced Research and Technology Development Program.

The overall emissivity of coal includes diffuse, broadband absorption in addition to peaks associated with specific functional groups. The broadband absorption of coal probably arises from electronic excitations of π electrons in the graphitic, aromatic bonds in the coal matrix (7-9). These electrons are loosely bound by the nuclei, and can absorb radiation over a continuous wavelength region which extends far into the infrared. However, the electrons are not entirely free from nuclear attractions, and their emission spectra would not necessarily be expected to follow Planck's law. Therefore, even the radiation from coal at wavelengths void of any identifiable functional groups may not be gray in its characteristics.

The literature cited above indicates that the spectral emission of coal particles at sizes of importance to pulverized coal combustors (50-150 μm) is potentially nongray and could depend in complicated ways on particle size, coal rank, temperature and extent of reaction. However, the emission would be expected to behave more like a graybody with increasing particle size, coal rank, temperature, and extent of reaction. Although all of the literature suggests that there is some size at which the coal particle emission is nongray, no study has been sufficiently definitive to quantify such a size for coals of various rank.

IMPACT OF NONGRAY COAL EMISSION ON COMBUSTION

The potentially nongray emission of coal particles impacts combustion in the areas of overall heat transfer and in the calculation of particle temperature from pyrometer measurements. An abnormally low emissivity due to nongray behavior could impact radiative heat transfer effects and either increase or decrease the rate of particle heat up, depending on the wall and particle temperatures and the optical depth of the combustion gases. Data collected in experimental and industrial combustors in which radiation is a signficiant contributor to the overall heat transfer to the particle may be subject to misinterpretation or error if an inappropriate emission spectrum is assumed. A particle emissivity which depends on particle size, coal type, and extent of burnout may be required to accurately calculate radiation heat transfer.

The sensitivity of two-color pyrometry to nongray emissions is illustrated in Figure 1 for three sets of wavelengths. The effective emissivities of the coal were assumed to be 0.9 and 0.8 at λ_1 and λ_2, respectively. The same results would apply for any emissivities with a ratio of 9:8. Pyrometry measurements at longer wavelengths are more sensitive to nongray emissivities. For example, if the ratios of emissivities are 9:8, a pyrometer operating at 5 and 6 μm would indicate the temperature of a 1500 K particle is over 3000 K and that a 2000 K particle would be measured as over 9000 K. This sensitivity provides practical motivation for determining the spectral emissivities of coal.

The experimental work reported in this paper analyzes spectral emissivities of various sizes and ranks of coal particles using emission FTIR techniques. Discussions of the experiment, the functional groups found in the spectra, and the size, burnout, and rank dependence of the findings follow.

EXPERIMENTAL PROCEDURE

Figure 2 is an illustration of the experimental equipment and optical layout employed in this study. A single layer of sized particles of coal and graphite were placed on a horizontal window of NaCl mounted in an aluminum ring. An electric strip heater was wrapped around the mount. The NaCl window was used because it can withstand higher temperatures without degradation and has a higher thermal conductivity than other windows that are transparent throughout the infrared spectrum. Temperatures as high as 400°C are possible

with this arrangement, although the temperatures used to obtain the spectra presented in this report seldom exceeded 200°C. The heated sample, optics, interferometer, and detector were enclosed in a nitrogen-purged container.

All coal samples were obtained from the Pennsylvania State University Coal Bank. The coal samples were ground in a nitrogen atmosphere, size classified by sieve trays, and some were dried in a nearly inert atmosphere at 305°C. Graphite samples were prepared similarly. All samples were visually examined and some were photographed after they were placed on the window to ensure they were well size-classified and formed a single layer.

The heated sample disc was movable in the horizontal plane, allowing the FTIR instrument to measure emission from the coal and from the graphite through the heated window, and from the heated window itself. The field of view of the system, calculated from geometric optics, was 6 mm in diameter at the sample plane. In practice, a portion of the signal from the edge of the collecting lens was lost, probably due to overfilling the detector.

The spectra in this paper were produced by averaging 800 interferograms, each with a resolution of 4 cm^{-1}. Approximately 5 minutes were required to obtain one spectrum under these condtiions. The large number of scans produced a high signal-to-noise ratio over most of the infrared region; peaks were observed with sufficient resolution to allow comparison with literature results. The emissivity of the coal (ϵ_s) was determined at each wavelength from the following equation:

$$\epsilon_s = \left(\frac{R_s/A_s - R_w/A_w}{R_g/A_g - R_w/A_w} \right) \epsilon_g \qquad 1)$$

where R is the measured intensity (radiance and system response), A is the emitting area, ϵ is emissivity, and subscripts s, g, and w refer to sample (coal), graphite, and window, respectively. The numerator in Equation 1 represents the energy flux emitted by the sample, accounting for background emission from the window. The quantity in parenthesis represents the emissivity of the sample relative to the emissivity of the graphite, and hence the right-hand side is multiplied by ϵ_g. This approach assumes that ϵ_g is constant over the wavelength spectrum. The spectral emissivity of the graphite particles was determined by correcting the measured intensity (R_g) for the system responsivity; the graphite particles exhibit nearly graybody behavior with a total emissivity of 0.92.

Emission FTIR is subject to interference from atmospheric absorption and emission. This effect was minimized in this experiment by measuring the emissivity of a reference body (graphite) of the same size and under the same conditions as the coal. This experimental procedure is roughly equivalent to individually calibrating the system responsivity for each measurement. Our experience was that this technique, combined with Equation 1, yielded spectra of superior quality to the more common approach of determining a single fixed system responsivity for several or all of the spectra.

The emitting areas of the graphite and coal and the transmissivity of the window were determined by measuring the extinction of a HeNe laser beam as it passed through a sample. The HeNe beam was expanded, and a central portion of the beam with the same diameter as the diagnostic area (6 mm) was used to minimize

errors from gradients in beam intensity. A power meter with a large detection area was used to measure the beam intensities and minimize errors due to scattered light.

The particle temperatures were assumed to be close to the window temperature, which were measured with a type K thermocouple placed on the window itself in the vicinity of the sample. The temperature at the center of the window was typically 5-10 Kelvins lower than that at the edge. However, the samples were located equidistant from the window edge to minimize errors due to temperature gradients. The data analysis can be completed without specifying the actual temperature so long as the window, coal, and graphite temperatures are equal.

The estimated accuracy of the measured emissivities is $\pm$ 5 relative percent. The major source of uncertainty in the emissivity was the determination of the actual emitting surface area. Although the HeNe laser could accurately measure the cross-sectional area of the samples within the nominal 6 mm sample, there were indications that a fraction of the signal from this area was not transmitted to the detector.

FEATURES OF THE COAL SPECTRA

Figure 3 is typical of the spectra collected in this study, showing the spectral emissivity of 40 μm diameter particles of a hvA bituminous coal (Pittsburgh #8, PSOC 1451). Peaks from various functional groups are identified in the figure. One small peak, at about 1850 cm^{-1}, is not typical of coal and has not yet been identified. The remaining peaks agree precisely with published spectra collected with a variety of instruments and techniques and validate the experimental procedure described above. Similar spectral features were found in the coals of other ranks. The spectra show maximum emissivities close to unity in regions of functional group absorption. The absorption of these peaks is typically high for submicron particles (8) and should not decrease with increasing particle diameter.

Some reaction of the coal was observed when the temperature was held above 150°C for 3 hours or longer. For example, the evolution of a peak at 1850 cm^{-1} is observed over a 2.0 hour period. Other coal reactions which were indicated by reductions in peak size include loss of hydrogen-bound hydroxyl and a small decrease in the aliphatic carbon. However, consecutive spectra taken within one hour of each other showed no losses and were reproducible at temperatures below 170°C. In any case, there was no evidence that a spectrum changed during the 5 minutes required to collect it.

DEPENDENCE OF EMISSIVITY ON SIZE, BURNOUT AND RANK

The spectral emissivity for 115 μm particles of a Pittsburgh seam (high-volatile A) bituminous coal is shown in Figure 4. A comparison of Figures 3-4 shows the dependence of spectral emissivity on coal particle size. The peaks are broader, the valleys are higher, and the emissivity in the featureless regions has increased for the larger particles, as anticipated. The emissivity of 115 μm particles of this bituminous coal varies from 0.7 to 1.0 over the range of 500 to 4100 cm^{-1}.

The spectral emissivities for 115 μm particles of a subbituminous coal and a lignite are shown in Figures 6 and 7. The subbituminous sample (PSOC-1445d) is a Western coal from the Blue #1 seam, and the lignite sample (PSOC-1507d) is a lignite from the Beulah Zap seam. These coal samples were sieved and aerodynamically classified under nitrogen to enhance size classification. These particular samples were not dried prior to analysis.

The dependence of emissivity on coal rank can be seen by comparing Figures 5-7. The nongray behavior of the lignite is more pronounced than in either of the higher rank coals, with emissivity varying from 0.57 to 1 0 in the region of the infrared indicated. However, little indication of aromatic spectral features is present in either of these samples. Interference from water in these undried samples is evident in the spectra.

A spectrum of partially devolatilized bituminous (PSOC 1451) coal appears in Figure 8. This sample was prepared by entraining the coal in a 1000 K inert gas stream in a down-fired, laminar flow reactor. The proximate volatile content of the parent coal is 40 % on a dry, ash-free basis. The weight loss of these samples has not yet been measured, but it is estimated that devolatilization was nearly completed when the sample was collected. The unreacted coal particles used in this analysis were those used to generate Figure 5. The dependence of particle emissivity on coal burnout can be seen by comparing Figures 5 and 8.

The emissivity of these particles is quite constant at 0.8 at wavenumbers above 1900 cm^{-1}. The aliphatic and hydroxyl groups, which were emitting strongly in the unreacting coal, appear to have either volatilized or reacted to form other compounds. However, a weak aromatic peak persists at 3000 cm^{-1}. The emissivity of the aromatic peaks between 500 cm^{-1} and 1900 cm^{-1} slightly exceeds that of the parent coal, possibly due to the formation of tar. Finally, the emissivity in featureless regions of the spectrum did not change appreciably from the parent coal.

IMPLICATIONS ON PYROMETRY AND RADIATIVE HEAT TRANSFER

The spectral emissivity shown in Figure 5 can be used to evaluate the potential impact of nongray emissions on pyrometry measurements. For example, a two-color pyrometer operating at 3333 and 2500 cm^{-1} (3 and 4 μm) would overestimate the temperature of a 1500 K particle by 200 K. A similar error would occur if the pyrometer operates at 3333 and 2000 cm^{-1} (3 and 5 μm). If the pyrometer were operating at 2000 and 1667 cm^{-1} (5 and 6 μm), it would underestimate the particle temperature by 700 K. Errors in pyrometry measurements due to nongray emissivities can be minimized by making one measurement at a short wavelength (around 1 μm) or increasing the separation between wavelengths, the former strategy being more effective than the latter. These trends are shown in Figure 1. However, signal strengths at typical combustion temperatures decrease sharply with decreasing wavelength in the near infrared and visible regions, requiring a judicious choice between acceptable signal-to-noise ratios and sensitivity to this type of error.

Total emissivities for use in radiative heat transfer calculation will depend in a complicated way on coal rank and on particle size, temperature, and degree of burnout. For high rank coals above 40 μm in size, the total emissivity could vary between 0 65 and near 1.0. Lignites have a wider variation in emissivity. The importance of these variations and the effect they have on heating rate depend primarily on the combustor configuration and flow field. In many instances, devolatilization may be completed before the particle reaches a high temperature, and only the optical properties of the residual char affect combustion behavior.

CONCLUSIONS

An emission FTIR experimental technique is used to study emission characteristics of coal particles. Coal particles in the size ranges between 40 and 115 μm show nongray behavior at wavelengths between 2.2 and 17 μm Spectral emissivities of high rank coals vary from 0.7 to 0.98. Spectral emissivities of lignites may be as low as 0 5 at some wavelengths. The particles generally are more gray as particle size, rank and extent

of burnout increase. The emissivity generally increases with increasing rank and particle size. As burnout increases, the particle emissivity can either increase, decrease, or remain constant, depending on the region of the spectrum being considered.

Pyrometry measurements in the 2.2 to 17 μm wavelength interval are subject to errors due to nongray effects. The errors in temperature measurement vary from a few hundred degrees to many thousands, depending on the wavelengths chosen. Operating one channel of the pyrometer at a short wavelength reduces the chance for error.

The effect of nongray emissions on heat transfer calculations will depend on the particular combustor and flow field being used. Total particle emissivities range from about 0.6 to 0.95 for 115 μm diameter particles, depending on particle temperature and coal rank. Smaller particles from low rank coals have lower emissivities. Partially devolatilized samples of bituminous coal emit as gray bodies over a large portion of the infrared spectrum, with emissivities of about 0.8.

REFERENCES

1. Brewster, M. Q., and Kunitomo, T. "The Optical Constants of Coal, Char, and Limestone," *ASME Transactions, 106, (1984).*
2. *Huntjens, F. J., and van Krevelen, D. W., Fuel, 33, (1954).*
3. *Solomon, P. R., Carangelo, R. M., Best, P. E., Markham, J. R. and Hamblen, D. G., "The Spectral Emittance of Pulverized Coal and Char," Twenty-first Symposium (International) on Combustion, Munich, West Germany, 1986.*
4. *Foster, P. J. and Howarth, C. R., "Optical Constants of Carbons and Coals in the Infrared," Carbon, 6 (1968).*
5. *Blokh, A., The Problem of Flame as a Disperse System, Halsted Press, (1974).*
6. *Cannon, C. G. and George, W. H., Proc. Conf. Ultrafine Structure of Coals and Cokes, BCURA, London, 1944.*
7. *Berry, R. S., Rice, S. A. and Ross, J. Physical Chemistry, Wiley, New York 1980.*
8. *van Krevelen, D. W., Coal, Elsevier, 1981.*
9. *Berkowitz, N., The Chemistry of Coal, Elsevier, 1985.*

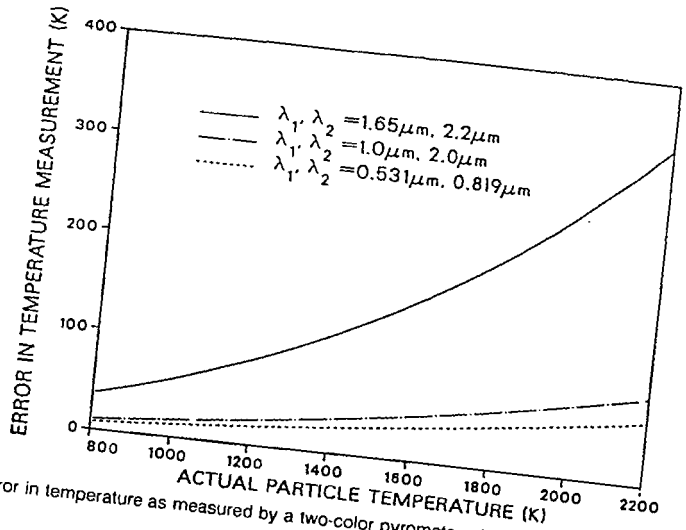

Figure 1. Error in temperature as measured by a two-color pyrometer when the emissivity ratio at λ_1 and λ_2 is 9·8.

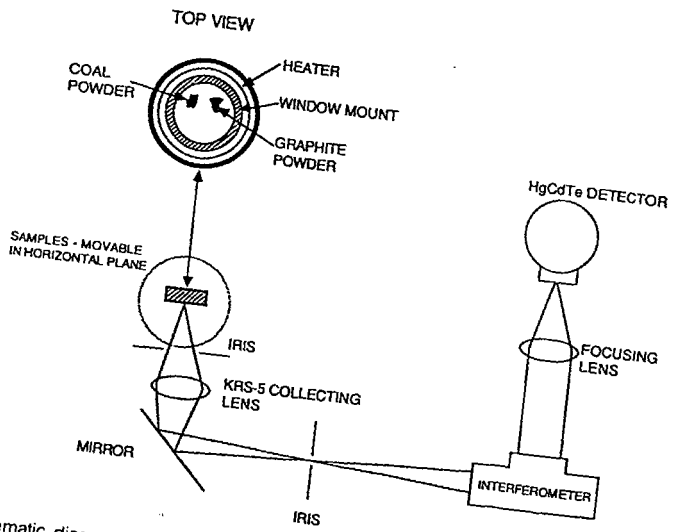

Figure 2. Schematic diagram of experimental facility for measurements of the spectral emissivity of coal particles.

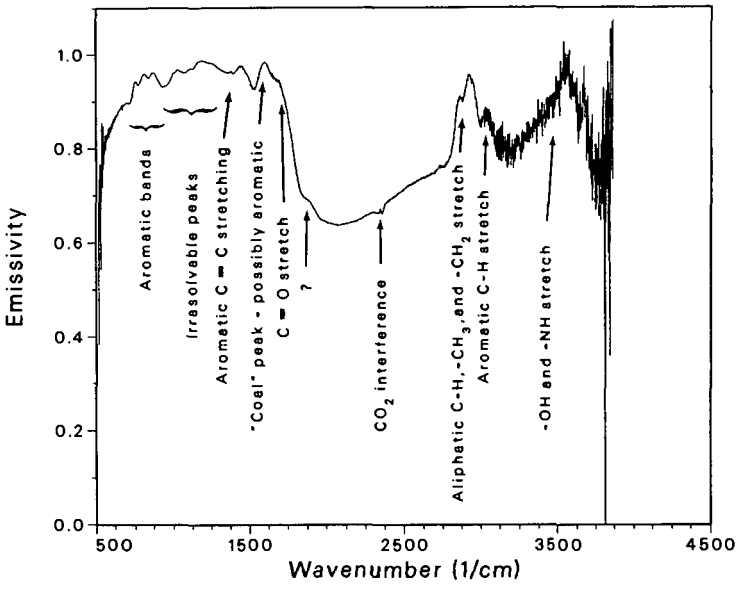

Figure 3. Spectral emissivity of 40 μm hvA bituminous coal (PSOC 1451) at 171°C, identifying peaks associated with various coal functional groups.

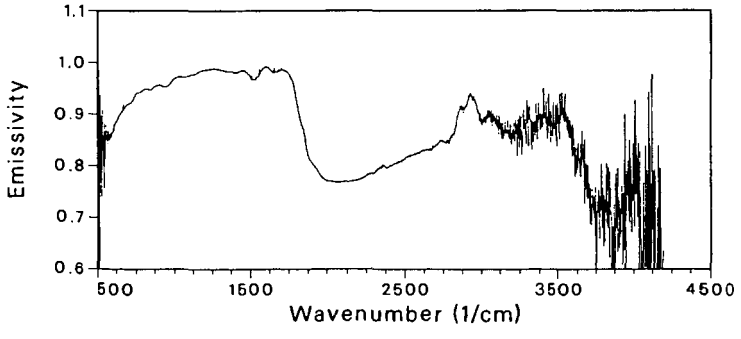

Figure 4. Spectral emissivity of 115 μm diameter hvA bituminous coal particles (PSOC 1451) at 182°C.

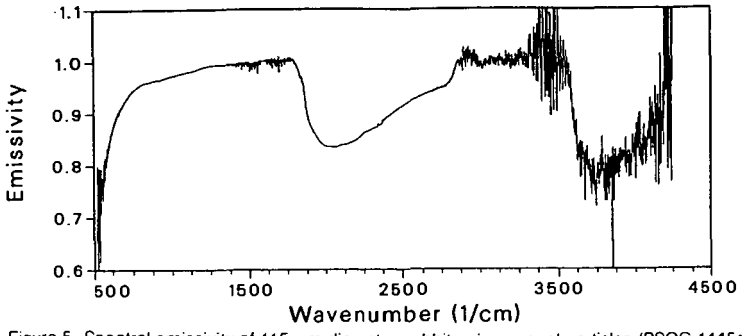

Figure 5. Spectral emissivity of 115 μm diameter subbituminous coal particles (PSOC 1445d) at 180°C.

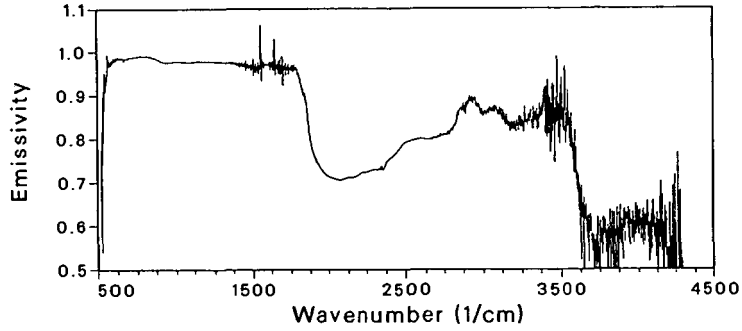

Figure 6. Spectral emissivity of 115 μm diameter lignite particles (PSOC 1507d) at 190°C.

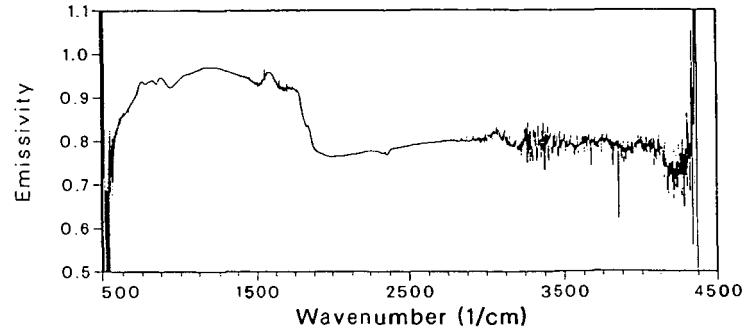

Figure 7. Spectral emissivity of 115 μm diameter hvA bituminous coal particles (PSOC 1451) at 182°C after partial devolatilization at 1000 K.

The Significance of Transport Effects in Determining Coal Pyrolysis Rates and Yields

Eric M. Suuberg
Division of Engineering
Brown University
Providence, R.I. 02912

INTRODUCTION

The recent search for robust but mathematically simple models of coal pyrolysis has led to many significant advances in the area of modeling the wide range of chemical reactions responsible for many key phenomena (gas release, tar formation). It has also become clear that transport phenomena cannot be disregarded in such models. There has emerged a debate concerning the role of heat transfer and various mass transfer processes in determining both the overall timescales of pyrolysis, and the compositions of products from these processes. Many of the earlier theories concerning the role of transport processes in coal pyrolysis were reviewed in various recent publications (Howard, 1981; Gavalas,1982; Suuberg,1985). It seems appropriate in the context of this symposium to review some recent developments and conclusions.

THE ROLE OF HEAT TRANSFER

THE HEAT OF PYROLYSIS

It is instructive to consider exactly what is meant by the term "heat of pyrolysis". This term has been used in many different ways by many different workers, and as a result there is some confusion about the magnitude of the term and whether it even warrants inclusion in any particular analysis. The various possible components of the heat of pyrolysis are:

1. The sensible enthalpy of heating the coal and its decomposition products to a particular temperature.
2. The enthalpy of the actual decomposition reactions.
3. The heat of vaporization of any condensed phase decomposition products that ultimately escape the particle by evaporation (i.e. not all tar molecules evaporate immediately when formed in the coal- they must diffuse first to a surface at which they can evaporate).

Some species essentially evaporate as they are formed (e.g. CO_2), and it is customary to lump the heat of evaporation and heat of reaction into a single term (the enthalpy of reaction) in those cases. Under the conditions of relevance in coal pyrolysis, only in the case of formation of the heavy tars will the distinction between steps 2 and 3 above be important.

Most, though not all workers in the field, have sought to distinguish between the contributions of items 1 and 2 to the heat of pyrolysis. Few workers have tried to distinguish between all three effects. Many of the experiments upon which estimates of the heat of pyrolysis are based simply are not designed so as to permit the distinctions to be drawn. for example, a calorimetric experiment in which a sample is pyrolyzed in the interior of a calorimeter (Davis,1924) will not take into account the heat effect due to item 3 above-in addition to the recondensation of tars inside the calorimeter, one will also have to generally contend with condensation of water and lighter oils as well. The corrections due to such condensation effects (which are

generally unlikely in actual pulverized gasification or combustion processes) may be difficult to make, even if the composition of the products is known. Other types of experimental systems have not lent themselves well to separation of sensible enthalpy and reaction enthalpy effects.Much of the difficulty derives from the fact that the enthalpy effects due to reaction and evaporation processes are small, and of the same order of magnitude as sensible enthalpy effects.

The work of Davis and Place(1924) is often cited as evidence that the heat of pyrolysis is small enough to neglect. These workers however pointed out several important facts:

1. The net heat of pyrolysis varies quite a bit with rank
2. The heat of pyrolysis that will be reported from any experiment depends upon the conditions under which pyrolysis is performed.
3. Related to the above, the heat effects of pyrolysis involve a series of endo- and exotherms which sum to the total heat of pyrolysis.

Davis and Place reviewed some earlier relevant literature that suggested many of the same uncertainties that are cited today--the variabilty of apparent heats of pyrolysis was large, with values ranging from 1060J/g endothermic to 837J/g exothermic.In their own calorimetric work, Davis and Place found apparent enthalpies of reaction that were in all cases less than 400J/g endothermic. The lower ranks of coal were observed to exhibit the largest endothermic reaction enthalpies, when a correction was applied to take into account the latent heat of condensation of water. Higher temperatures seemed to promote the occurrence of more endothermic processes, as did the addition of hydrogen to the gaseous environment (Davis, 1924). It is important to note that this work involved slowly heated samples, pyrolyzed at low temperatures. No corrections were included for the latent heat of evaporation of tars. It is not clear how reliably these results can be extrapolated to the higher temperature and heating rate conditions of pulverized coal processing.

Some years later, Mahajan et al.(1975) studied the same problem using differential scanning calorimetric techniques (DSC). They obtained qualitatively similar results to those of Davis and Place, in that their enthaplies of pyrolysis ranged from about 80J/g exothermic to 250J/g endothermic.

Burke and Parry (1927) provided a different viewpoint to the study of this problem. They distilled coals to 870K in an open retort, such that all the tar that was evolved from the bed could escape in the vapor state, and thus at least some contribution of a latent heat of tar evaporation was included. Also, they did not separate out sensible enthalpy effects from reaction enthalpy and latent heat effects in their experiments. The net heat consumed by a Colorado subbituminous coal was 1109J/g, while a Pittsburgh high volatile bituminous coal consumed 946J/g. An attempt was made by the authors to factor out the contribution of sensible enthalpy, and they concluded that the values of 16J/g (Pitt. coal) and 198J/g (Colo. coal), both exothermic, were in reasonable agreement with the results of Davis and Place (not including latent heat corrections). These values demonstrate very well the difficulty that will be encountered in any attempt to factor out sensible enthalpies by calculation--the values are sufficiently large compared to the reaction enthalpy terms that the calculations cannot be considered reliable, except to provide an order of magnitude estimate.

A number of subsequent attempts have been made to estimate the heats of pyrolysis, including the sensible enthalpy terms. The work of Kirov (1965) has led to a correlation for the heat of coking:

$$Q(J/g)=343+1.20T$$

where T is the temperature of coking in centigrade (see also Sharkey and McCartney,1981). The work of Lee (1968) suggests a similar correlation:

$$Q(J/g) = [0.728 + 8.28 \times 10^{-4} T + (1.38 + 2.30 \times 10^{-3} T) V](T-21)$$

where V is the volatile matter content of the coal. Using either method yields fair agreement with the earlier cited data of Burke and Parry, though obviously the first correlation's use is restricted to coking coals. The success of such simple correlations must again be ascribed to the fact that sensible enthalpy terms dominate the estimates.

The above viewpoint is apparently at odds with that of Baum and Street (1971), who imply that there is a distinct heat of vaporization which has to be supplied in order for volatiles to escape. The value cited in that work is 627.9J/g of coal, and is based upon the authors' own experiments. This value is considerably higher than most estimates of the heat of reaction, and most estimates of the latent heat of tar volatiles evaporation. It is difficult to obtain data on the latent heats of vaporization of the heavy tars of interest in coal pyrolysis. Briggs and Popper (1957) proposed a correlation for the latent heat of vaporization of "tar oils" which has the form:

$$\Delta H_v(J/g) = S_{20}(485.8 - 0.598 T_b)$$

where S_{20} is the specific gravity of the tar at 20°C and T_b is its boiling point in K. The difficulty in using this correlation for coal tars is that their boiling points are not well known. To address the need for estimates of tar vapor pressures, Unger and Suuberg (1983) developed a crude correlation as a function of molecular weight alone, based on limited data on the vapor pressure of ring compounds with sidechains:

$$P^o(atm) = 5756 \exp(-255 M^{.586}/T)$$

where M is the molecular weight of the tar, T is the temperature in K.A "typical" tar molecular weight of 600 (see Unger and Suuberg,1984) would be estimated to have T_b=1250K. This is clearly outside the range of applicability of the above correlation. Instead, applying the Clausius-Clapeyron equation to the vapor pressure equation itself yields

$$\Delta H_v(J/g) \approx 2120 M^{-0.414}$$

Another similar analysis by Homann(1976) yields:

$$\Delta H_v(J/g) \approx 1960 M^{-0.346}$$

These correlations give estimates for a typical tar species of 600 molecular weight of ΔH_v=150 to 215J/g.To compare this value to earlier cited estimates of heats of pyrolysis, one can note that tar yields represent typically no more than 1/4 to 1/3 the mass of a particle; thus the latent heat of tar evaporation is a sink of order 70J/g coal if all tar had M=600. A lower assumed molecular weight does not change the conclusion much--e.g. M=200 gives a latent heat requirement of about 100J/g coal. Thus, the latent heat term is of the same order of magnitude as the measured heats of pyrolysis reported earlier.

Estimation of the reaction enthalpy term is also quite difficult, because there are so many possible contributing processes. Attempts at estimation of this term by measurement of pyrolysis products, and then comparing heats of combustion of starting material and final products have been difficult (one such attempt is described in Suuberg et al.,1978). All that can be said as a result of these efforts is that at high heating rates (1000K/s), the general conclusion of near-thermoneutrality seems to still apply. Recent experiments in which the temperature response of a coal-loaded, electrically heated wire grid is carefully examined seem, upon rough calculation, to support the earlier estimates of the magnitude of the heat of pyrolysis as well (Freihaut and Seery,1983).

HEAT TRANSFER CONTROL

It appears, then, that the weight of evidence still favors the viewpoint that the heat of pyrolysis is dominated by sensible enthalpy requirements for heating the particle to reaction temperature, and that the reaction enthalpy requirements and

latent heat requirements are both modest (not more than 1/4 to 1/2 of the total). This means that the classical analysis of heat conduction in a solid, in which the reaction enthalpy and latent heat effects are neglected, still appears reasonable. Under these circumstances, the characteristic time for diffusion of heat in the absence of reaction heat effects is:

$$t_H = O\ (r^2/\alpha)$$

where r is the particle radius and α the thermal diffusivity of the particle; the latter is temperature dependent, but of order $1x10^{-3}cm^2/s$ at low temperatures (Badzioch et al.,1964). The timescale for pyrolysis reaction may be defined:

$$t_R = O\ [A\ exp(-E/RT)]^{-1}$$

Naturally, the absence of heat transfer limitations during reaction is assured by $t_R >> t_H$, or, approximately:

$$r < [0.1\alpha\ exp(E/RT)/A]^{-1}$$

This is similar to the criterion suggested by Gavalas(1982). The selection of A and E has a significant effect on the conclusions, however. A conservative approach might involve selection of these parameters for the fastest reaction of interest. This might be, for example, the initial CO_2 evolution reactions in pyrolysis of lignites, for which $A=2.1x10^{11}s^{-1}$, E=151kJ/mol (Suuberg et al., 1978). Selecting as an arbitrary ambient temperature 1650K, heat transfer limitations are apparently not important only if r<0.05μm! For a temperature of 1200K, r<0.4μm. These radii are considerably smaller than those calculated by Gavalas, and serve to illustrate the importance of the choice of kinetic constants in such analyses. Recognizing that coal pyrolysis involves a broad spectrum of reactions, each with its own kinetic parameters, the so-called distributed activation energy models have been developed. If one uses a mean activation energy to obtain a characteristic timescale for <u>all</u> pyrolysis reactions, the conclusions change markedly. For example, Anthony et al. (1975) report that for pyrolysis of a lignite, the mean value of E is 204kJ/mol, $A=1.07x10^{10}s^{-1}$. With these kinetic parameters, such a timescale analysis suggests that at 1200K, r<30μm is sufficient to assure the absence of heat transfer limitations. It is also apparent that the choice of temperature has an effect on the conclusions reached above. It may legitimately be asked if the use of the ambient temperature as the characteristic temperature may not be too conservative, since the particle may be well below this temperature during much of the process. This aspect will be clarified below.

Another analysis that has been suggested as a method of determining whether heat transfer limitations are significant is that due to Field et al.(1967). In this analysis, the magnitude of the temperature gradient in a particle is examined (generally the center of the particle is cooler than the ambient). The magnitude of the surface to center temperature gradient is, conservatively:

$$\Delta T = rq/2k$$

where q is the surface heat flux and k the thermal conductivity of the particle. For a 100μm particle being radiatively heated in a 1650K environment, the maximum value of q is roughly $40W/cm^2$. Taking a typical $k=2.5x10^{-3}W/cm\text{-}K$ (Badzioch et al.,1964), the maximum ΔT is calculated to be roughly 40K. Field et al. cite this as evidence that pulverized fuel particles, which are generally less than 100μm in diameter, may be taken as essentially spacially isothermal. For any particle that does have an internal temperature gradient, the relative rates of pyrolysis at its surface and center may be estimated from:

$$k_s/k_c = exp[(1/T_c - 1/T_s)E/R] \approx exp[\Delta TE/RT_s^2]$$

where the k's are rate constants and the subscripts c and s refer to center and surface, respectively. For E=151kJ/mol and the above ΔT=40K, apparently the ratio is 1.65 at

T_s=1200K or 1.3 at 1650K. Thus the rates throughout the particle are reasonably constant. The ratio increases with increasing E and decreasing T_s, but even if E=204kJ/mol and T_s=1200K, the ratio is but 2. Thus the rates at the surface and center of the particle are both of the same order of magnitude in such a case.

The two different methods of analysis apparently yield contradictory conclusions about the importance of internal heat transfer limitations for particles in the 30-100μm size range. This is symptomatic of the confusion that exists concerning the role of heat transfer in pyrolysis. The resolution of the apparent conflict comes in closer examination of the criteria for heat transfer control.It was noted above that the use of the ambient temperature in the calculation of characteristic times for reaction was unduly conservative. The more reasonable approach involves examining the timescales for pyrolysis of both the center and the surface of the particle, given an estimate of the actual ΔT in the particle. Only if the latter quantities differ significantly is there an important internal heat transfer limitation.

There has also been some confusion caused by imprecise discussion of the role of external heat transfer limitations. For the purposes of illustration, assume that pyrolysis can be modeled as a simple first order process with a rate:

$$dM/dt=-A\ M\ \exp(-E/RT)$$

where M is the mass of unpyrolyzed material remaining at time t. Further, assume that the particle heats up at a linear rate dT/dt=B, then it has been shown numerous times that it is possible to approximately integrate the rate expression above to obtain conversion ($1-M/M_0$) as a function of maximum temperature achieved (T_m):

$$(1-M/M_0) \approx \exp[-A\ \exp(-E/RT_m)[t_i+RT_m^2/EB]] \qquad \text{(Eqn. A)}$$

where t_i is the time of any isothermal period during which the particle is held at T_m. Since the conversion as a function of time is determined by B, which in turn is a function of external heat transfer rate, this has in some cases been interpreted as an example of an "external heat transfer limitation". But it should be noted that chemical kinetics do indeed play a role in determining the time necessary to achieve complete conversion. Also, the case in which B is infinite can be recognized as the familiar case of complete chemical rate control.

RELEVANCE FOR PULVERIZED COAL DEVOLATILIZATION

From a simple heat balance, the surface heat flux to particles being uniformly heated at a constant rate B(K/s) must be given by:

$$q = d\rho c_p B/6 = dkB/6\alpha$$

where d is the particle diameter. Assuming B=1000K/s, d=75μm, and previously cited values, q=3.1W/cm^2, which implies that ΔT=2.4K. Thus the particles are essentially uniform in temperature and the many experiments on pulverized particles heated at these rates (common for heated grids) would be expected to be governed by the nonisothermal kinetic expressions of the form of eqn. A. These experiments then do indeed yield information on true kinetics. If particles of 1mm are examined under the same conditions, ΔT ≈ 430K, and the interpretation of the results in the same terms is questionable at best.

At a nominal average heating rate of B=10^{4}K/s, 75μm particles would support a temperature gradient of about 24K, given the present assumptions. At a surface temperature of 1000K, the rate of a pyrolysis reaction with 210kJ/mol activation energy would be 1.8 times as high on the surface as in the center of the particle. However, it should be noted that about 60% of the mass of the particle is within 10μm of its surface. At a depth of 10μm, the temperature will lag that of the surface by only 12K, and the reaction rate will be only 35% lower. Such small differences in rate would normally not be apparent within the uncertainty of measurements in such high heating

rate experiments.

Only at particle average heating rates of 10^5K/s and above do internal heat transfer limitations become important for typical pulverized-size particles. The surface heat fluxes implied by such heating rates are 300W/cm^2 for 75 μm particles, and temperature gradients of order 240K may be expected, based on the above analysis. It is then not surprising that at such fluxes (produced by laser radiation), Hertzberg and Ng (1987) observed a particle diameter effect on devolatilization half-life, with particles in the range 51-105μm. At 100W/cm^2 irradiation, the effect of particle size was seen to be very small. The implication is that for typical pulverized coal particles heated at ordinary rates (<10^4K/s or <100W/cm^2 flux), pyrolysis can be well described by a standard Arrhenius rate expression that accounts for the temporal nonisothermality of the process (e.g. equations of the form of A), without specifically accounting for internal heat transport limitations.

At higher fluxes, pyrolysis is expected to exhibit the observed "wave" character, in which the onset of reaction coincides with penetration of the thermal wave into the coal. The temperature of the wavefront is easily predicted from equation A, setting t_i=0 and assuming for example that the appearance of the wavefront coincides with about 50% conversion for the most facile reaction (kinetic parameters cited earlier for such a reaction were A=2.11x10^{11}s^{-1}, E=151kJ/mol). For a heating rate B=10^5K/s, the calculated T_m=960K is the apparent wavefront temperature. For B=10^4K/s, which would yield pyrolysis wave behavior only in "large" particles according to the above analysis, the apparent wavefront temperature is calculated to be about 870K, in good agreement with the observations of Hertzberg and Ng.

It may be concluded further that for high fluxes or large particles, that the standard Arrhenius kinetic expressions, combined with standard heat transfer analysis, are sufficient to describe the rate of pyrolysis, without the need to resort to the concept of a "decomposition temperature". As shown above, such a temperature would be a function of heating rate and reaction kinetics, and thus not a fundamental quantity.

More detailed analyses of the combined heat transfer-reaction processes in coal are still hampered by the lack of good thermodynamic and transport data on these systems. Even if the data on heats of reaction and latent heats were available, construction of a robust heat transfer model would have to wait for simultaneous development of a mass transfer model, since the location of evaporative tar loss (and thus the associated heat sink) would not necessarily coincide with the location of the reaction front in the coal.

THE ROLE OF MASS TRANSFER

There has recently appeared an extensive review on modeling of mass transfer limitations in coal pyrolysis (Suuberg,1985), and this material will not be repeated here. Since the publication of that review, there have been a number of developments in understanding the processes involved, and these will be briefly summarized. As usual, a distinction is drawn between processes that are mainly of relevance in softening coals, and those that occur in the porous structure of non-softened coals.

Mass Transfer in Softening Coals

A major unresolved issue is that concerning the handling of bubble transport of volatiles, and whether it plays the dominant role in determining tar yields during pyrolysis. It has been shown that models which involve transport of volatiles out of the coal through bubbling-type behavior can indeed capture many essential features of the process (Lewellen,1975;Oh et al.,1983,1984). However, it has also been shown that a simple model in which liquid phase diffusion controls the rate of escape of tars might also explain the tar yield data equally well for pulverized particles (Suuberg and

Sezen, 1985). Thus it is not yet clear what role the bubbles must play in transporting tars. Further work on this latter model has, not surprisingly, revealed that liquid phase diffusion is most likely not fast enough to explain tar yields from particles much larger than about 100μm, under high heating rate conditions. Consequently, the evidence favors at least some role of bubbles in helping remove the tar from the particles, since no other convective mechanism is evident. A new, semi-empirical model of bubble transport has recently been proposed.

This new model of bubble transport of tar volatiles proposes that the tars are carried out in small bubbles that are nucleated by light gaseous species and oils. Solomon (1987) proposes an analogy of cups on a conveyor belt-each cup can carry out a certain amount of tar, as determined by the saturation vapor pressure of the tar. The effect of pressure on tar yields is seen through the effect on the size of the cups-the higher the pressure, the smaller the cup, and the less tar it transports. The smaller the rate of tar transport out via the cups, naturally the longer the residence time of tars in the particle, and the greater the opportunity for yield reducing cracking/coking reactions. More formally, each bubble is assumed saturated with respect to all tar species present in the surrounding liquid. Assuming ideal vapors and liquid solutions, the total number of moles of a tar species of molecular weight M_i in a bubble is:

$$n_i = P_i v_b/RT = P_i^0 x_i (v_g+\Sigma v_j)/RT$$

where v is a volume, with the subscript b referring to the whole bubble, g referring to the fixed gases in the bubble, and j to the volume contribution of the tars themselves. The quantity x_i is a liquid phase fraction of species i and P_i^0 is its vapor pressure.

The rate of escape of the tar species i is governed by the rate of escape of bubbles from the particle, which is given, at constant pressure, by the total volumetric rate of escape of bubbles:

$$dN_i/dt = (P_i^0 x_i/RT)dV_t/dt = (p_i^0 x_i/P_{tot})dN_t/dt$$

where N_i is the same as n_i multiplied by the total number of bubbles that escape, and V_t is the total volume of all volatiles, which is related by the ideal gas law to the total number of moles of volatiles, N_t. The pressure P_{tot} is the prevailing ambient pressure.

The implied inverse pressure dependence of the rate of tar escape is the same as was previously noted based on another model-one in which film diffusion controls the rate of tar escape (Suuberg et al.,1979,1985; Unger and Suuberg,1981). In that model, the rate of tar escape was given for a particle of radius R by:

$$dN_i/dt = 4\pi RDx_i P_i^0/RT$$

where the inverse pressure dependence is implicit in the vapor phase diffusion coefficient of tar in the gas film around the particle (D).Either model will predict a variation of molecular weight distribution with pressure (see Suuberg et al.1985).

Solomon (1987) has noted that the rate of escape of the bubbles from the coal should be linked to the size of the particle, the viscosity of the coal melt (μ), and the pressure difference between bubble and ambient (ΔP). The latter effect is proportional to dN_t/dt, leading to the following suggested empirical form for the rate of tar escape:

$$dN_i/dt = (c_1 P_i^0 x_i/RP_{tot}\mu)(dN_t/dt)[1/(P_{tot}+\Delta P)]$$
$$= (c_1 P_i^0 x_i/RP_{tot}\mu)(dN_t/dt)\{1/[P_{tot}+c_2(dN_t/dt)]\}$$

As of this writing, equations of this form are being tested.

Porous Transport

There has been relatively little new work in this area since it was last reviewed, except that the standard pore transport analysis has been extended to account for temporal nonisothermality (Bliek et al.,1985). This area awaits further work on the question of how pressures affect yields of tar volatiles in non-softening coals. It

seems clear that pressure affects the rate of convection and diffusion. But is this in turn affecting tar yields by virtue of an impact on the residence times of vapor phase species in pores (affecting the residence time for vapor phase cracking/coking) or by virtue of an impact on evaporation rate of tar species (affecting the residence time for condensed phase cracking/coking)? It also appears necessary to clarify what role if any, is being played by microporous transport, under reactive conditions. The distinction between micropore transport and bulk diffusion remains hazy.

ACKNOWLEDGEMENT

The support of the USDOE through grant DE-FG22-85PC80527 is gratefully acknowledged.

REFERENCES

Anthony,D.B., J.B.Howard,H.C.Hottel, and H.P.Meissner, 15th Symp.(Int.)on Comb.,p1303 The Combustion Institute,1975.

Badzioch,S., D.R.Gregory,M.A. Field, Fuel,43,267 (1964).

Baum,M.M. and P.J. Street,Comb. Sci. and Tech.,3,231 (1971).

Bliek,A.,W.M.vanPoelje,W.P.vanSwaaij,and F.P.van Beckum, AIChEJ,31,1666 (1985).

Briggs,D.K. and F.Popper,Trans.Inst.Chem.Engr.(London),35,369 (1957).

Burke,S.P.and V.F. Barry, I&EC,19, 15 (1927).

Davis,J.D., I&EC,16(7),726 (1924).

Davis,J.D. and Place,P.B.,I&EC,16(6),589 (1924); Fuel,3,434 (1924).

Field,M.A.,D. Gill,B.Morgan, and P. Hawksley, BCURA Monthly Bulletin,31(3),81 (1967).

Freihaut, J.D., and D.J.Seery, ACS Division of Fuel Chem. Prepr., 28(4), 265 (1983)

Gavalas,G.R.,Coal Pyrolysis,Elsevier, New York,1982.

Homann,K.H., 16th Symp.(Int.) on Comb.,p717,The Combustion Institute, 1977.

Hertzberg,M. and D.Ng, paper presented at NATO Advanced Research Workshop on Fundamentals of Physical Chemistry of Coal Comb., Les Arcs, France,1986.

Kirov,N.Y., BCURA Monthly Bulletin,29(2),33 (1965).

Lee,A.L.,ACS Div.Fuel Chem. Prepr.,12(3),19 (1968).

Lewellen,P.C., M.S. Thesis, Dept. of Chem. Eng., M.I.T., Cambridge, Mass., 1975.

Mahajan,O.P., A. Tomita, J.R. Nelson, and P.L. Walker, Jr.,ACS Div. Fuel Chem. Prepr.,20(3),19 (1975).

Oh,M.,W.A. Peters, and J.B. Howard, Proc.Int. Conf. on Coal Sci.,p483, IEA (1983).

Oh,M.,J.B.Howard,and W.A.Peters,"Modeling Volatiles Transport in Softening Coal Particles, paper presented at the AIChE annual meeting, November,1984.

Sharkey,A.G.,Jr. and J.T. McCartney,in Chem. of Coal Utilization, Second Suppl.Vol. M.A. Elliott,Ed.,p198,Wiley, New York,1981.

Solomon, P.R., AFR,Inc., personal communication (1987).

Suuberg,E.M., in Chemistry of Coal Conversion,R.Schlosberg,Ed., p67,Plenum, 1985.

Suuberg,E.M.,W.A.Peters, and J.B.Howard,17th Symp.(Int.)on Comb.,p117, The Comb. Inst., 1979.

Suuberg,E.M.,W.A. Peters, and J.B. Howard,I&EC Proc. Des. and Dev.,17,37 (1978).

Suuberg,E.M. and Y. Sezen, Proc.Int. Conf. on Coal Sci.,p913, Pergamon (1985).

Suuberg,E.M., P.E. Unger and W.D.Lilly, Fuel,64,956 (1985).

Unger,P.E. and E.M.Suuberg,18th Symp.(Int)on Comb.,p1203,The Comb. Inst.,1981.

Unger,P.E. and E.M.Suuberg,Fuel,63,606 (1984).

Unger,P.E. and E.M.Suuberg,ACS Div.FuelChem.Prepr.,28(4),278 (1983).

DIFFUSIONAL CONTRIBUTIONS TO VOLATILE RELEASE IN PYROLYZING COAL PARTICLES

Mahendra K. Misra and **Robert H. Essenhigh**

The Ohio State University
Department of Mechanical Engineering
206 West 18th Avenue
Columbus, Ohio 43210

SUMMARY

Unsteady state calculations of pyrolyzing coal particles under slow and rapid heating have been compared with experimental data for particles in the size range 20 microns to 4 mm; and the comparison has shown, contrary to common assumption, that the diffusional escape is an important factor in determining the pyrolysis times for all particle sizes. Pyrolysis times for particles greater than 500 microns range from 0.1 to 10 sec; and for particles less than 100 microns range from 0.05 to 0.5 sec with an unexpected overlap in times. This overlap is accounted for by assuming that the diffusion coefficients for the escaping volatiles are about 100 times greater (order of 10^{-1} cm^2/sec) for the larger particles than for the smaller particles (order of 10^{-3} cm^2/sec). This result raises the questions regarding purely kinetic interpretations of pyrolysis rate data for small particles.

1. INTRODUCTION

In this paper we present comparison between calculated and experimental values of pyrolysis times in the particle size range 20 microns to 4 millimeter. The experimental data were taken from the literature [1-17]. The calculations are based on an unsteady state heat transfer model, with escape of volatiles after chemical release inside the particle controlled, we assume, by diffusional or convective escape. The model and a number of other results, notably temperature-time distribution through a particle and profiles of pyrolysis release rates, have been described earlier [18,19]. In this paper, we summarize the elements of the model, the equations and computational procedures; focus here is on the contribution of the diffusional escape.

In past evaluation of pyrolysis studies, it has generally been concluded that escape of pyrolysis products from particles below about 100 microns is so fast as to be effectively "instantaneous". This conclusion, however, is not in fact supported by values of pyrolysis times in the larger data base now available; and, as we shall show in this paper, we have only been able to obtain good agreement between the experimental values and our predictions for the times, and their variations with diameter, when a significant diffusional escape factor is included in the calculations, even for particles as small as 20 microns. This result clearly raises questions regarding the purely kinetic interpretations of pyrolysis rate data for small particles presented in the past.

2. EXPERIMENTAL DATA BASE

A data base consisting of total pyrolysis times under different conditions from the literature was compiled for comparison with our predicted values of times and their variation with particle size. The experimental methods used included (mostly) Drop-tube and or Heated-grid experiments, carried out in inert atmospheres; and from experiments performed in the presence of oxidizing atmospheres (mostly flame experiments). A summary of the data along with the investigators and the nature of experimentation is given in Tables 1 and 2 and in Figure 1.

In the majority of the measurements on captive particles [1] (650 values) coal particles were cemented to silica fibers and burnt between two electrically heated, flat spiral coils. The burning times of the volatiles were determined using a PE

cell, and these times were assumed to be equal to the pyrolysis times. The experiment was carried out for 10 different coals with particle sizes in each case ranging from about 700 microns to 4 millimeters. For each coal type, the pyrolysis time and the particle size could be related by the expression

$$t_v = K_v d_o^n \qquad (1)$$

The values of K_v and n are listed in Table 2; it can be seen that the values of K_v are about 100 c.g.s units, and the index n is about 2. A similar result was obtained by Kallend and Nettleton [2] in a similar experiment, but with the particles mounted on thermocouples. Figure 1 shows that the results of the two experiments are in close agreement. Other data are for particles smaller than 200 microns and have been taken mostly from some of the Drop-tube, Heated-grid,and flame experiments. The pyrolysis times in these cases have been defined as the time period between the 1% and 99% loss by weight of the ultimate yield of Volatile Matter. The data collected are for heating rates ranging from 10^3 to 10^5 deg.K/sec.

Figure 1 shows an unexpected overlap in the pyrolysis times between the larger particles below 100 microns, and the smaller of the captive particles above 700 microns. A continuous curve from a single equation passing approximately through all data sets would be a dog-leg, which is unexpected. Also unexpected is the apparently strong dependence of pyrolysis times on diameter below 100 microns, contrary to the common belief. It is these two aspects of behavior, in particular, that we are addressing in this paper.

3. PHYSICAL MODEL

The model is that of a particle plunged into an enclosure whose temperature is rising. Heat transfer can be jointly by conduction (convection) and by radiation. The calculations show that, in the case of the captive particles, radiation only dominated over conduction for particles greater than 2 millimeters. The behavior is an unsteady state so that temperature non-uniformities can exist through the particles, resulting in variable rates of pyrolysis at different points. Escape of the products is treated phenomenologically as a diffusional process, either actual, and dependent on concentration differences, or effective, where the actual driving force may be pressure differences. One objective here is to establish the actual or apparent diffusion coefficients required to account for the experimental results as targets for further mechanistic analysis using approximate pore and pore-tree models.

4. MATHEMATICAL MODEL

4.1 Governing Equations:

Heat Transfer: For a particle in a thermal enclosure, the dimensionless equations for heat transfer inside and outside the particle, describing the change in temperature, θ, as a function of radial distance, η, and time, τ, is

$$R_c \, \partial\theta/\partial\tau = (1/\eta^2)\,\partial[\eta^2 \, \partial\theta/\partial\eta]/\partial\eta - C \exp(-1/\theta)\delta \qquad (2)$$

where the dimensionless groups are defined as

$$\theta = RT/E \qquad (3)$$

$$\tau = (\alpha_p / r_o^2)t \quad ; \qquad \eta = (r/r_o) \qquad (4)$$

$R_c = 1$ for $\eta < 1$; $R_c = \alpha_p / \alpha_a$ for $\eta > 1$.

and $\delta = 1$ for $\eta < 1$; $\delta = 0$ for $\eta > 1$

The quantity C is

$$C = \sigma k_o r_o^2 \Delta H(V_o - V)/\lambda_p \qquad (5)$$

The initial conditions are (for $\tau = 0$):

for $0 < \eta < 1$, $\Theta = 1$ and for $1 < \eta < \infty$, $\Theta = \Theta_o$

and the boundary conditions are

$$[\partial\theta/\partial\eta]_{\eta=0} = 0 \quad ; \quad [\Theta]_{\eta=\infty} = 0 \qquad (6)$$

At the particle surface, the temperatures of the particle and the gas are equal, and the heat flux to the particle is the sum of heat flux from the gas and the net radiative heat flux from the enclosure. This shows that the radiation appears as a boundary condition at the particle surface.

Pyrolysis is assumed to be a first-order, one-step reaction; and the heat absorbed in pyrolysis is

$$h = \sigma k_o \exp(-E/RT)(\Delta H)(V_o - V) \qquad (7)$$

Mass Transfer: The governing equations for the diffusion of volatiles through the coal matrix are of the same form as the heat transfer equations and can be written as

$$\partial m/\partial t = (1/r^2)\partial(r^2 D_i \partial m/\partial r)/\partial r + \delta m_g \qquad (8)$$

where

$$m_g = \sigma_p k_o \exp(-E/RT)(V_o - V) \qquad (9)$$

and

$\delta = 1$, $D_i = D_p$ for $r < r_o$; $\delta = 0$, $D_i = D_a$ for $r > r_o$.

The boundary conditions are

$$[\partial m/\partial r]_{r=0} = 0$$
$$[D_p \partial m/\partial r]_{r=r_o} = [D_a \partial m/\partial r]_{r=r_o} \text{ and } m_{part} = m_{air} \qquad (10)$$
$$\partial m/\partial r = 0 \text{ at } r = \infty.$$

Mass Loss: At any instant of time, the flow rate of volatiles out of the particle surface is

$$m_t = 4\pi r_o^2 D_p [\partial m/\partial r]_{r=r_o} \qquad (11)$$

and the total mass loss over a period t is given by

$$M_t = \int_0^t m_t dt \qquad (12)$$

4.2 Solution Procedures Eqn.(2) is transformed into appropriate difference forms for solution using a Central difference approximation on the spatial coordinate, and a backward difference approximation on the time co-ordinate. Equations 2 and 8 can be written in the common dimensionless, difference form

$$-\eta_{i-1/2}^2 \Theta_{i-1}^{n+1}/\Delta\eta^2 + [R_c \eta_i^2/\Delta\tau + (\eta_{i+1/2}^2 + \eta_{i-1/2}^2)/\Delta\eta^2]\Theta_i^{n+1} -$$
$$\eta_{i+1/2}^2 \Theta_{i+1}^{n+1}/\Delta\eta^2 = \delta C \eta_i^2 \exp(-1/\Theta_i^n) + \eta_i^2 R_c \Theta_i^n/\Delta\tau \qquad (13)$$

The relevant difference equations were then solved numerically using a fully implicit backward-difference scheme and iterating at each time step for the non-linear terms.

5. RESULTS

5.1 Pyrolysis Times: Instantaneous Escape of Volatile Matter: The results of earlier attempts to predict pyrolysis times and their variation with particle size with only chemical kinetics in the model and diffusional escape omitted, are presented in Fig. 2, with the experimental data of Fig. 1 included for comparison. These results are obtained by selecting $D_1 = \infty$.

It can be seen in Figure 2 that the predicted curve is sigmoid shaped -- largely under-predicting times for large particles (greater than 2000 microns) and over-predicting times for small particles. The shape of the curve also indicates that pyrolysis times are insensitive to the variation of particle size in the small size range. The predictions are good for a small intermediate range (1000 microns to 2000 microns) but this agreement would now appear to be fortuitous. Increasing the kinetic rate by decreasing the activation energy from 30 kcal/mole to 25 kcal/mole did not improve the predictions. Though the pyrolysis times were reduced, the calculations still over-predicted times for small particles and under-predicted for large particles.

Examination of the calculated temperatures of the small particles during pyrolysis showed that the particles would heat up to a final temperature of about 950 K without significant pyrolysis, and that they then pyrolyzed at constant temperature; it was also found that the temperature gradients within the small particles (less than 500 microns) were insignificant. At constant temperature, pyrolysis is a volumetric process; the pyrolysis time then depends on the temperatures of the particles, and is independent of the particle size. The final temperatures attained by the small particles were about the same. This is the source of the flattening of the predicted curve in the small particle range. Although this supports the common belief that pyrolysis being independent of particle size below 100 microns, it is clearly contrary to the facts. It also emphasizes the inadequacies of the assumptions, and the need to re-examine them (following).

The under-prediction of pyrolysis times for large particles indicated by Fig. 2 suggests that escape time is important for such particles. When this assumption was incorporated in the model equations, it was then found to be applicable to all particle sizes.

5.2 Pyrolysis Times: Diffusion of Pyrolysis Products: With diffusional escape included in the model, the results illustrated in Fig. 3 were obtained. Figure 3 shows 3 diffusional escape times, using diffusion coefficients of 10^{-3}, 10^{-4}, 10^{-5} cm^2/sec. To obtain the lines shown, an adjustment to the velocity constant coefficients was necessary; otherwise, the calculated times were high by one or two orders of magnitude. The fit was obtained by reducing the activation energy from 30 to 12 kcal/mole. This is substantially below the values quoted for individual reactions in a multiple pyrolysis model, but it is of the typical magnitude found by fitting a single step to multiple reactions [3].

The fit then shows that the separate trends of the large and the small diameters can be accounted for by attributing the major differences to the different diffusion rates. Second order variations, to the extent that these can be identified, can be attributed to differences in the actual kinetics.

6. DISCUSSION

The principal problem then remaining is to account for the very different diffusion coefficients (by two orders of magnitude) between the "large" and the "small" particles. It is not a matter of oxidizing or non-oxidizing ambient atmospheres since the small particle group include some values obtained in flames. Two possible explanations can be advanced. One factor that can be significant is the extent of swelling. It is now generally agreed that (small) particles heating rapidly swell only marginally or not at all [19]. With the large particles, swelling was very evident -- with the exception of the anthracite -- with measured swelling

factors average 1.5 for all the coals (except for the anthracite) [20]. This explanation, however, does not account for the behavior of the non-swelling anthracite whose large-particle pyrolysis times do not differ significantly from those of the bituminous coal.

If swelling is not responsible for the differences we must postulate, it would seem, some unidentified differences in the mechanical properties of the coals that are solely particle size dependent, and which include anthracite. One such property could be microcracks in all particles greater than about 100 microns so that the VM escape rate in smaller particles can be diffusion-dominated, generating the left-hand data set of Fig. 3. If the VM escape through the microcracks of larger particles was then instantaneous, all pyrolysis times of particles about 100 microns would level off at about 0.5 sec.,and the line would become horizontal in the right-hand segment of the graph. If escape through the microcracks is not instantaneous, and is governed by some form of diffusion mechanism, the line to the right would then rise with particle size, as it does in fact.

The same qualitative result is obtained if we assume, alternatively, an array of microcracks at all particle sizes, and with microcrack size diminishing with particle size.

This is all hypothetical at this time but it does indicate the line of thinking that would appear to be necessary at this time to account for the observed results.

7. CONCLUSIONS

1. The experimental data on the variation of pyrolysis times with diameter clearly show influence of particle size over the size range 20 to 4000 microns.
2. The dependence of pyrolysis times on diameter is interpreted at this time as being due to the influence of (diffusional) escape in the pyrolysis mechanism. This is in agreement with conventional views of pyrolysis greater than 100 microns; but it contrary to those views for particles less than 100 microns.
3. A single line or band drawn (empirically) through all the data has a sigmoid (dog-leg) shape that cannot at this time be accounted for, theoretically, by any model that excludes diameter-dependent parameter coefficients.
4. The two extreme segments of the sigmoid curve can be predicted by arbitrarily assuming that values of a diffusion coefficient governing VM escape differ by two orders of magnitude.
5. Mechanistic reasons for any such difference in diffusion coefficients are not clear at this time. Some factors, such as the influence of the composition of the ambient atmosphere (oxidizing or non-oxidizing) can apparently be ruled out. A tentative explanation in terms of microcracks is suggested but this needs to be tested by approximate analytical developments and physical examinations.

ACKNOWLEDGEMENTS

We would like to acknowledge the support of Mr. J. Hickerson, Department of Energy (contract # DE-AC22-84PC-70768) and Dr. D. Seery, United Technologies Research Center (contract # 101404) in funding this project.

NOMENCLATURE

D_a : diffusion coeff. in air (cm^2/s)
D_p : diff. coeff. in particle (cm^2/s)
E^a : activation energy (kcal/mole)
k^p : rate constant (s^{-1})
k_o : preexponential factor (s^{-1})
m : mass conc. of VM (g/cc)
m_g^o : volatile generation rate ($g/cm^3 s$)
q_r : radiative heat flux ($cal/cm^2 s$)

r	: radial distance (cm)	r_o	: radius of a particle (cm)
R	: gas constant (cal/mole deg.K)	t	: time (s)
T	: Temperature (deg.K)		
T_o	: Initial Temperature (deg.K)	V	: volatile yield (%)
V^o	: ultimate volatile yield (%)	α_a	: thermal diffusivity in air
α^p	: thermal diffusivity in particle	ΔH	: heat of reaction (cal/gram)
η^p	: dimensionless radial distance	λ_a	: thermal conductivity of air
λ^p	: thermal conductivity of coal	σ_a	: density of air (gram/cc)
σ^p	: density of coal (gram/cc)	τ	: dimensionless time
θ^p	: dimensionless temperature		

REFERENCES

1. Essenhigh, R.H. The Influence of Coal Rank on the Burning Times of Single Coal Particles. Journal of Eng. for Power. 1963. pp.183-190.

2. Kallend, A.S and Nettleton, M.A. Burning of Volatile Matter from Single Coal Particles. Sonderdruck aus >> Erdol und Kohle. Erdgas. Petrochemie <<. 19. 1966. pp.354-356.

3. Anthony, D.B; Howard, J.B; Hottel, H.C and Meissner, H.P. Rapid Devolatilization of Pulverized Coal. Fifteenth Symp. (Int.) on Combustion. 1975. pp. 1303-1317.

4. Desypris, J; Murdoch, P and Williams, A. Investigation of the Flash Pyrolysis of some Coals. Fuel. 61. 1982. pp.807-816.

5. Howard, J.B and Essenhigh, R.H. Pyrolysis of Coal Particles in Pulverized Fuel Flames. I & EC Process Design and Development. 6. 1967. pp.74-84.

6. Kobayashi, H; Howard, J.B and Sarofim, A.F. Coal Devolatilization at High Temperatures. Sixteenth Symposium (Int.) on Combustion. 1977. pp.411-425.

7. Maloney, D.J and Jenkins, R.G. Coupled Heat and Mass Transport and Chemical Kinetic Rate Limitations during Coal Rapid Pyrolysis. Twentieth Symposium (International) on Combustion. 1984. p.1435-1443.

8. Niksa, S; Heyd, L.E; Russel, W.B and Saville, D.A. On the Role of Heating Rate in Rapid Coal Devolatilization. Twentieth Symp. (Int.) on Comb. 1984. pp.1445-1453.

9. Nsakala, N.Y; Essenhigh, R.H and Walker, P.L. Studies on Coal Reactivity: Kinetics of Lignite Pyrolysis in Nitrogen at 808 deg.C. Combustion Science and Technology. 1977. pp.153-163.

10. Peters, W and Bertling, H. Kinetics of the rapid Degasification of Coals. Fuel. 44. 1965. pp.317-331.

11. Scaroni, A.W; Walker, P.L and Essenhigh, R.H. Kinetics of Lignite Pyrolysis in an Entrained-Flow, Isothermal Furnace. Fuel. 60. 1981. pp.71-76.

12. Seeker, W.R; Samuelsen, G.S; Heap, M.P and Trolinger, J.D. The Thermal Decomposition of Pulverized Coal Particles. Eighteenth Symposium (International) on Combustion. 1981. pp.1213-1226.

13. Smoot, L.D; Horton, M.D and Williams, G.A. Propagation of Laminar Pulverized Coal-Air Flames. Sixteenth Symposium (Int.) on Combustion. 1977. pp.375-387.

14. Solomon, P.R; Serio, M.A; Carangelo, R.M and Markham, J.R. Very Rapid Coal Pyrolysis. Fuel. 65. 1986. pp.182-193.

15. Thring, M.W and Hubbard, E. H. Radiation from Pulverized-Fuel Flames. Paper#4 . Second conference on Pulverized Fuel, Nov.,1957. Inst. Fuel, London. 1957.

16. Ubhayakar, S. K; Stickler, D. B; Von Rosenberg, C. W and Gannon, R. E. Rapid Devolatilization of Pulverized Coal in Hot Combustion Gases. Sixteenth Symposium (International) on Combustion. 1977. pp.427-436.

17. Misra, M. K, M.S Thesis, Department of Mechanical Engineering, The Ohio State University, Columbus, Ohio. 1987.

18. Misra, M. K and Essenhigh, R. H, Pyrolytic Behavior of Coal Particle: Effect of Unsteady State Heating and Temperature Gradients. Paper# 10 presented at the Spring Technical Meeting, Central States Section, The Combustion Institute, Chicago, IL. May, 1987.

19. Discussion at the Workshop on "Fundamentals of Physical-Chemistry of Pulverized-coal combustion" held at Les Arcs (Bourg-Saint Maurice), France. July-August, 1986.

20. Essenhigh, R. H and Yorke, G. C, Reaction Rates of Single Coal Particles: Influence of Swelling, Shape, and Other Factors. Fuel. vol 44, May, 1965. pp.177-189.

Table 1: Pyrolysis Times from Drop-tube (DT) Heated -grid (HG), and Flame (F) Experiments.

Investigators	Particle Size (microns)	Heating Rate (deg.K/sec)	Pyrolysis Time (sec)	
Anthony [3]	53-83	10^4	0.1	HG
		3×10^3	0.3	
Nsakala [9]	64	9×10^3	0.2	DT
Niksa [8]	125	10^2-10^4	0.5	HG
Kobayashi [6]	37-44	$> 10^4$	0.1	DT
Howard [5]	< 200	10^4	0.2	F
Smoot [13]	21	10^4	0.05	F
Thring [15]	< 100	-	0.1	F
Ubhayakar [16]	< 74	$> 10^5$	0.011	DT
Seeker [12]	80	10^5	0.08	Shock Tube
Peter [10]	1200	200	3.5	-
Desypris [4]	126	-	0.5	HG
	44	-	0.5	
Maloney [7]	62	-	0.17	DT
Solomon [14]	53-74	10^4	0.064	DT
	44-74	3×10^4	0.02	
	44-74	4×10^4	0.023	

Table 2: Values of the volatile combustion constants (K_v and n).
(Source: Ref. 1)
(The errors in K_v are between 2 and 5% , the errors given against n are in percentage.)

COAL	VM% (d.a.f)	K_v (c.g.s units)	n
1. Stanllyd	9.9	44.6	1.82 ± 4.18%
2. Five ft.	14.9	80.0	2.32 ± 4.37%
3. Two ft. Nine	28.8	120.0	2.63 ± 3.33%
4. Red Vein	23.3	86.6	2.19 ± 4.22%
5. Garw	30.6	96.8	2.06 ± 2.14%
6. Silkstone	41.5	91.6	2.19 ± 3.86%
7. Winter	39.3	93.6	2.24 ± 3.18%
8. Cowpen	40.2	91.4	2.15 ± 3.28%
9. High Hazel	40.7	134.0	2.28 ± 2.79%
10. Lorraine	40.2	98.9	2.14 ± 2.55%

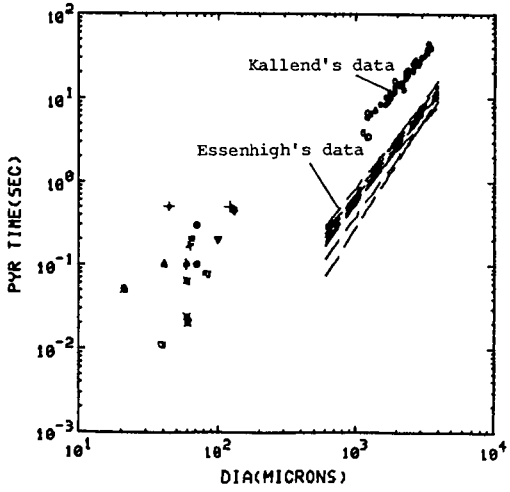

Figure 1. Experimental values of variation of total pyrolysis times with particle size. Values are listed in Tables 1 and 2.

● Anthony. ■ Nsakala. ♦ Niksa. ▼ Howard. ▲ Kobayashi. ✱ Smoot. ♦ Thring. ▼ Solomon. ✕ Maloney. ✚ Desypris. ○ Ubhayakar. ○ Peters. ▽ Seeker.

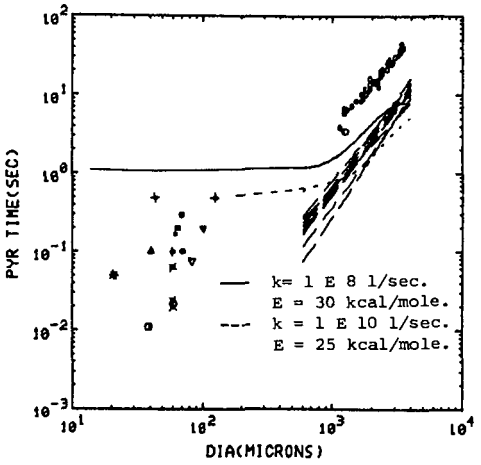

Figure 2. Comparison of the calculated and experimental variation of pyrolysis times with particle size. The calculations do not include the diffusional escape of VM.

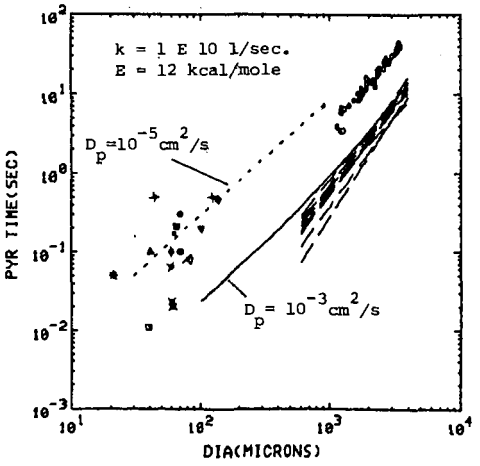

Figure 3. Comparison of calculated and experimental variation of pyrolysis times with particle size. The calculations include the diffusional escape of VM.